



Hebei loess section in the Anyemaqen Mountains, northeast Tibetan Plateau: a high-resolution luminescence chronology

Chongyi, E.; Sohbaty, Reza; Murray, Andrew Sean; Buylaert, Jan-Pieter; Liu, Xiangjun; Yang, Long; Yuan, Jie; Yan, Wenting

Published in:
Boreas

Link to article, DOI:
[10.1111/bor.12321](https://doi.org/10.1111/bor.12321)

Publication date:
2018

Document Version
Peer reviewed version

[Link back to DTU Orbit](#)

Citation (APA):

Chongyi, E., Sohbaty, R., Murray, A. S., Buylaert, J-P., Liu, X., Yang, L., Yuan, J., & Yan, W. (2018). Hebei loess section in the Anyemaqen Mountains, northeast Tibetan Plateau: a high-resolution luminescence chronology. *Boreas*, 47(4), 1170-1183. <https://doi.org/10.1111/bor.12321>

General rights

Copyright and moral rights for the publications made accessible in the public portal are retained by the authors and/or other copyright owners and it is a condition of accessing publications that users recognise and abide by the legal requirements associated with these rights.

- Users may download and print one copy of any publication from the public portal for the purpose of private study or research.
- You may not further distribute the material or use it for any profit-making activity or commercial gain
- You may freely distribute the URL identifying the publication in the public portal

If you believe that this document breaches copyright please contact us providing details, and we will remove access to the work immediately and investigate your claim.



Hebei loess section in the Anyemaqen Mountains, northeast Tibetan Plateau: a high-resolution luminescence chronology

Journal:	<i>Boreas</i>
Manuscript ID	BOR-056-2017.R2
Manuscript Type:	Original Article
Date Submitted by the Author:	12-Apr-2018
Complete List of Authors:	<p>E, ChongYi; Qinghai Normal University, Key Laboratory of Physical Geography and Environmental Processes of Qinghai Province; Nordic Laboratory for Luminescence Dating, Department of Geoscience, Aarhus University</p> <p>Sohbati , Reza ; Nordic Laboratory for Luminescence Dating, Department of Geoscience, Aarhus University; Technical University of Denmark, Center for Nuclear Technologies</p> <p>Murray, Andrew; Aarhus University, Department of Geosciences</p> <p>Buylaert, Jan-Pieter; Nordic Laboratory for Luminescence Dating, Department of Geoscience, Aarhus University; Center for Nuclear Technologies, Technical University of Denmark,</p> <p>Liu, Xiangjun; Qinghai Institute of Salt Lakes, Chinese Academy of Sciences</p> <p>Yan, Wenting; Qinghai Normal University, Key Laboratory of Physical Geography and Environmental Processes of Qinghai Province</p> <p>Yuan, Jie; Qinghai Normal University, Key Laboratory of Physical Geography and Environmental Processes of Qinghai Province</p> <p>Yang, Long; Qinghai Normal University, Key Laboratory of Physical Geography and Environmental Processes of Qinghai Province</p>
Keywords:	loess, Tibetan Plateau, luminescence dating, quartz and K-feldspar

1
2
3 Hebei loess section in the Anyemaqen Mountains, northeast
4 Tibetan Plateau: a high-resolution luminescence chronology
5
6

7 CHONGYI E, REZA SOHBATI, ANDREW S. MURRAY, JAN-PIETER BUYLAERT,
8
9 XIANGJUN LIU, LONG YANG, JIE YUAN AND WENTING YAN
10

11
12
13
14 E, C., Sohbati, R., Murray, A. S., Buylaert, J.-P., Liu, X., Yang, L., Yuan, J. & Yan, W.:
15
16 Hebei loess section in the Anyemaqen Mountains, northeast Tibetan Plateau: a
17
18 high-resolution luminescence chronology. *Boreas*...

19
20
21 The extensive aeolian deposits of the Tibetan Plateau represent important
22
23 environmental archives, recording information about the past interplay
24
25 between the Asian monsoon and Westerlies and the link between dust
26
27 accumulation and Quaternary glaciations. In northeast Tibetan Plateau,
28
29 mantles of sandy loess form a distinct belt lying between 3500 and 4500 m
30
31 a.s.l. on the east-facing slopes of the Anyemaqen Mountains. However, there
32
33 is little chronological information about the loess deposits in this region. This
34
35 study provides a detailed chronology for loess formation in the region using
36
37 luminescence dating. A total of 29 samples were collected from an 8-m thick
38
39 homogeneous loess section at Hebei (HB) for dating sand-sized (63-90 μm)
40
41 quartz and K-feldspar fractions using optically stimulated luminescence (OSL)
42
43 and infrared stimulated luminescence (IRSL and pIRIR) signals, respectively.
44
45 The resulting quartz and feldspar ages are in good agreement over the last 40
46
47 ka; beyond this (i.e., $D_e > 120$ Gy), the quartz age is underestimated, and the
48
49 pIRIR₁₇₀ feldspar ages are considered more reliable. The HB loess section
50
51 records continuous environmental information from ~50 to ~30 ka, i.e.
52
53 throughout Marine Isotope Stage (MIS) 3. Mass accumulation rates (MAR)
54
55 varied considerably over this period with increased dust accumulation around
56
57 ~38 ka and after ~32 ka; in between, and at the beginning of MIS 3 (50-40 ka)
58
59 the dust accumulation rate was ~50% lower. Finally, the HB section also
60
61 records a MIS 2 hiatus of ~17 ka duration, probably resulting from deflation.

1
2
3 This study implies that loess deposition on the Tibetan Plateau is
4 predominantly an interglacial/interstadial phenomenon and the TP may be
5 deflating at the same time as the CLP is accumulating, at least during MIS 2.
6
7
8
9

10
11 *Chongyi E (echongyi@163.com), School of Geographical Science, Qinghai*
12 *Normal University, 810008 Xining, P.R. China; Nordic Laboratory for*
13 *Luminescence Dating, Department of Geoscience, Aarhus University, DTU*
14 *Risø Campus, DK-4000 Roskilde, Denmark; Center for Nuclear Technologies,*
15 *Technical University of Denmark, DTU Risø Campus, DK-4000 Roskilde,*
16 *Denmark; and Qinghai Province Key Laboratory of Physical Geography and*
17 *Environmental Process, Qinghai Normal University, 810008 Xining, P.R. China;*
18 *Andrew S. Murray, Nordic Laboratory for Luminescence Dating, Department of*
19 *Geoscience, Aarhus University, Risø DTU, DK-4000 Roskilde, Denmark; Reza*
20 *Sohbati and Jan-Pieter Buylaert, Nordic Laboratory for Luminescence Dating,*
21 *Department of Geoscience, Aarhus University, Risø DTU, DK-4000 Roskilde,*
22 *Denmark, and Center for Nuclear Technologies, Technical University of*
23 *Denmark, DTU Risø Campus DK-4000 Roskilde, Denmark; Long Yang, Jie*
24 *Yuan and Wenting Yan, School of Geographical Science, Qinghai Normal*
25 *University, 810008 Xining, P.R. China; and Qinghai Province Key Laboratory*
26 *of Physical Geography and Environmental Process Qinghai Normal University,*
27 *810008 Xining, P.R. China; XiangJun Liu, Qinghai Institute of Salt Lakes,*
28 *Chinese Academy of Sciences, 810008 Xining, P.R. China; received 13th*
29 *August 2017, accepted 12th April 2018.*
30
31
32
33
34
35
36
37
38
39
40
41
42
43
44

45 The Tibetan Plateau (TP) is the most extensive and most elevated mountain
46 plateau on Earth. Because of its sensitivity to global climatic change it has
47 been referred to as the Third Pole (Qiu 2008). The extensive aeolian deposits
48 on the TP are important environmental archives of past environmental
49 changes, especially the interplay between the Asian monsoon and the
50 Westerly system (Fig. 1A) and the link between dust accumulation and
51 Quaternary glaciations. As a result, understanding the timing of loess
52
53
54
55
56
57
58
59
60

1
2
3 deposition is crucial to reconstructing both the development of the Quaternary
4 landscape in Tibet and the changes in the broader Asian Quaternary climate
5 (Lehmkuhl *et al.* 2000; Lu *et al.* 2004; Li & Li 2006; Owen *et al.* 2006; Sun *et al.*
6 2007; Lai *et al.* 2009; Stauch *et al.* 2012; Lehmkuhl *et al.* 2014).
7
8
9

10 There are significant differences between the basal age of loess in interior
11 TP and adjacent areas. For example, the Xining loess on the northeast TP
12 (NETP), a stretch of the Chinese loess plateau, has a basal age of ~2.0 Ma at
13 an elevation of 2300 m a.s.l. (Lu *et al.* 2007), whereas the loess on the east TP,
14 including the Ganze loess with an elevation of 3480 m a.s.l. and the loess-like
15 Chendu clay, have a basal age of 0.8 Ma (Fang *et al.* 1996; Yang *et al.* 2010).
16 Most of the existing loess in the interior of Tibet, with a thickness of 1–3 m and
17 lying above 3000 m a.s.l., has accumulated since the last deglaciation i.e.
18 13–14 ka (Sun *et al.* 2007; Kaiser *et al.* 2010; Lu *et al.* 2011; Liu *et al.* 2012;
19 Stauch *et al.* 2012; Qiang *et al.* 2013; Yu & Lai 2014; Zhang *et al.* 2015a).
20 Sporadic and discontinuous LGP (Last Glacial Period) loess strata are
21 distributed in Gonghe Basin and Qilian Mountain (Zhang *et al.* 2015a; Qiang *et al.*
22 2016), and some >70 ka loess is sandwiched between alluvial gravels (Sun
23 *et al.* 2007; Liu *et al.* 2012). The lack of loess associated with full glacial
24 conditions is believed to be a result of either sparse vegetation cover, or the
25 erosion of loess during the beginning of each interglacial (Sun *et al.* 2007). In
26 addition, loess sedimentation is thought to be discontinuous before ~13 ka
27 (Zhang *et al.* 2015a), which limits its contribution to understanding the climate
28 change on TP during glacial periods. It is thus important to test these
29 hypotheses by investigating more loess sections on the TP, especially in the
30 inner TP.
31
32
33
34
35
36
37
38
39
40
41
42
43
44

45 In October of 2014, a detailed field investigation was carried out in the
46 source region of Yellow River. There, mantles of sandy loess form a distinct
47 belt with a thickness of 1–20 m covering an elevation ranging between 3500
48 and 4500 m a.s.l. on the east-facing slopes of the Anyemaqen Mountains and
49 the terrace of Yellow River. The homogeneous aeolian loess in Hebei county
50 reaches a thickness of 8 m without any visible intercalated palaeosols, and so
51 the Hebei section offers the opportunity of obtaining high resolution
52
53
54
55
56
57
58
59
60

1
2
3 palaeoenvironmental information. However, there is little chronological
4 information available for the loess deposits in this region. The purpose of this
5 study is to provide a high-resolution chronology for loess formation in the
6 region using luminescence dating.
7
8
9

10 11 12 **Hebei section and sampling** 13

14
15 The Hebei loess section (34°43'13" N, 100°48'29" E, 3669 m a.s.l.) is situated
16 on the east-facing slopes of the Anyemaqen Mountains and the north bedrock
17 terrace of Yellow River (Fig. 1B). The Anyemaqen Mountains are formed within
18 a zone of transpression at the easternmost end of the Kunlun fault system,
19 rising from the surrounding peneplain at 4000 m a.s.l., and reaching a
20 maximum altitude of 6282 m a.s.l. (Roberts 2012). Moraines, erratics, cirques,
21 trough valleys and other glacial landforms are widespread in the study area,
22 and three terminal moraines in the eastern Anyemaqen Mountain have been
23 dated to 45.5, 16 and 9 ka (Thrasher *et al.* 2009). The Hebei loess section is
24 located ~100 km to the east of the Anyemaqen glaciers; the dominant wind
25 direction in the region is from the west, indicating that Hebei loess is probably
26 'cold loess'. The present climate in the study area is dominated by the Asian
27 monsoon system. Most of the precipitation falls in summer, and a cold and dry
28 continental air mass prevails in winter. The mean annual temperature,
29 precipitation and evaporation in Tongde weather station 60 km away from the
30 section are 0.5 °C, 440 mm and over 1350 mm, respectively. The landscape of
31 the study area is mostly vegetated by alpine meadow and subalpine steppe.
32
33
34
35
36
37
38
39
40
41
42
43

44 The loess at the Hebei section is ~8 m thick and directly overlies
45 pluvial-fluvial gravels. Except for the darker modern soil layer in the top ~10 cm,
46 the whole section is yellowish, loose and homogenous. The average grain-size
47 is coarse silt, between 34 and 45 μm . There is no obvious calcic horizon or
48 carbonate concretion in the whole loess stratum. Only a small number of snail
49 fossils were found at depths >6 m. Twenty-nine luminescence samples were
50 taken from the Hebei section at 20-30 cm intervals in October 2014. All OSL
51
52
53
54
55

1
2
3 samples were obtained by hammering steel tubes (25 cm long cylinders with a
4 diameter of 5 cm) into a freshly dug vertical section. The tubes were then
5 covered and sealed with cotton, and finally wrapped in plastic and tape to
6 avoid light exposure. At 615 and 720 cm, two groups of well-preserved snails
7 were sampled and sent to Beta Analytics Inc. for accelerator mass
8 spectrometry (AMS) radiocarbon (^{14}C) dating.
9
10
11
12
13
14
15

16 **Sample preparation and measurement**

17
18 All the samples were prepared and measured in the Nordic Laboratory for
19 Luminescence Dating. Under subdued orange light, the outer 2-3 cm ends of
20 tube samples were removed and reserved for environmental dose rate
21 measurement. The inner part of the sample was wet sieved to the grain-size
22 range 63-90 μm . This fraction was treated with HCl (10%) and H_2O_2 (10%) for
23 20 min. to remove any carbonates and organic material, and 10% HF for 40
24 min. to clean the grains. The treated material was floated in an aqueous heavy
25 liquid solution ('Fastfloat', $\rho = 2.58 \text{ g cm}^{-3}$) to separate quartz-rich and K-rich
26 feldspar fractions. Finally, the quartz-rich fraction was further treated with
27 concentrated HF (i.e. 40%) for 60 min. to remove any remaining feldspar
28 contamination and the outer alpha-irradiated layer. Any fluoride contamination
29 was removed using 10% HCl for 20 min. After each step the samples were
30 washed with deionised water.
31
32
33
34
35
36
37
38
39

40
41 Quartz and K-rich feldspar grains were mounted as large aliquots (8 mm) in
42 a monolayer on 9-mm-diameter stainless steel discs (quartz) and cups
43 (feldspar) using silicone oil. All measurements were carried out on standard
44 Risø TL/OSL DA-20 readers (Bøtter-Jensen *et al.* 2010). OSL signals from
45 quartz were stimulated by blue LEDs emitting at 470 nm with a power density
46 of $\sim 80 \text{ mW cm}^{-2}$ at sample position and measured through a 7.5-mm Hoya
47 U-340 glass filter. IRSL signals from K-feldspar were stimulated using IR LEDs
48 with peak emission at 870 nm and a power density of $\sim 135 \text{ mW cm}^{-2}$ at sample
49 position and detected through a BG3/BG39 blue filter combination. Beta
50
51
52
53
54
55

1
2
3 irradiations used a $^{90}\text{Sr}/^{90}\text{Y}$ source mounted on the reader and calibrated for
4 both discs and cups using 180–250 μm calibration quartz grains (Hansen *et al.*
5 2015). The heating rate was 5 $^{\circ}\text{C s}^{-1}$ throughout.
6
7
8

9 **Environmental dose rate measurement**

10
11
12 The outer 2-3 cm ends of tube samples were used to evaluate the
13 environmental dose rate. Most samples (24) were measured by high resolution
14 gamma spectrometry (Murray *et al.* 1987). The dose rates for the remaining 5
15 samples with small amounts of material (<30 g) were estimated using
16 inductively coupled plasma mass spectrometry (ICP-MS). The material for high
17 resolution gamma spectrometry was homogenized by grinding (<200 μm),
18 ignited at 450 $^{\circ}\text{C}$ for 24 hours to remove organic matter and cast in wax to
19 prevent ^{222}Rn loss and to provide a reproducible counting geometry. The solid
20 disc-shaped sample (>30 g of dry sample) was then stored for at least 3 weeks
21 before measurement to allow ^{222}Rn to build up to equilibrium with its parent
22 ^{226}Ra . The resulting radionuclide concentrations (Table 1) were converted into
23 infinite matrix dry dose rates using the conversion factors of Guérin *et al.*
24 (2012). The cosmic ray contribution was calculated following Prescott & Hutton
25 (1994), and a water content of 10 \pm 5% was assumed to apply throughout the
26 burial period. For quartz, an internal dose rate of 0.01 \pm 0.002 Gy ka $^{-1}$ was
27 assumed after Vandenberghe *et al.* (2008). For K-feldspar, an internal beta
28 dose rate was calculated based on an assumed ^{40}K content of 12.5 \pm 0.5%
29 (Huntley & Baril 1997; Zhao & Li 2005) and an assumed ^{87}Rb content of
30 400 \pm 100 p.p.m. (Huntley & Hancock 2001). A small internal alpha contribution
31 of 0.10 \pm 0.05 Gy ka $^{-1}$ was also included from internal ^{238}U and ^{232}Th based on
32 the measurements by Mejdahl (1987). The resulting total dose rates do not
33 vary significantly with depth (Table 1).
34
35
36
37
38
39
40
41
42
43
44
45
46
47
48
49
50
51

52 **Luminescence characteristics**

53 *Quartz*

1
2
3 The purity of quartz fractions was examined using the OSL–IR depletion ratio
4 test (Duller 2003). Three aliquots were measured from each sample. The
5 average OSL–IR depletion ratio was 0.96 ± 0.005 ($n = 87$), implying that any
6 feldspar contamination of the OSL signal from these samples is negligible. A
7 standard quartz OSL single-aliquot regenerative (SAR) dose protocol was
8 used for D_e measurements (Murray & Wintle 2000; Wintle & Murray 2006). Fig.
9 2A shows the dose-response and (inset) stimulation curves for one of the
10 samples. The OSL signal was rapidly bleached to background level within two
11 seconds (Fig. 2A) and is dominated by the fast component. The net quartz
12 OSL signal used for calculations was derived from the initial 0.32 s of the
13 signal (first two channels) minus an early background from the following two
14 channels i.e. 0.32 to 0.64 s (Ballarini *et al.* 2007; Cunningham & Wallinga
15 2010).

16
17
18 In order to select the appropriate preheat conditions for D_e determination,
19 natural (Fig. 2B) and dose-recovery preheat-plateau (Fig. 2C) tests were
20 conducted for three samples from the top (153001, depth 10 cm), middle
21 (153013, depth 400 cm) and bottom (153029, depth 760 cm) of the section.
22 The preheat temperature prior to the measurement of natural and regenerated
23 signals varied from 160 to 300 °C with 20 °C increments, and the cut-heat
24 temperature preceding the measurement of the test-dose signal was generally
25 40 °C (i.e. 160 - 260 °C) below the preheat temperature except for preheat
26 temperatures of 160 and 180 °C, for which the cut-heat temperature was kept
27 at 160 °C. For sample 153001 there is a D_e plateau from 180 to 280 °C (Fig.
28 2B). A D_e plateau also appears from 180 to 240 °C for samples 153013
29 and 153029, while at >240 °C, D_e values increase steadily with elevated
30 temperature (Fig. 2B).

31
32
33 In dose-recovery preheat-plateau tests, fresh aliquots from the same
34 samples were bleached twice with blue light for 100 s at room temperature,
35 separated by a pause of 10 ks. Then, a known laboratory beta dose close to
36 the expected D_e (based on an estimate determined as part of the purity test)
37 was given to these aliquots and measured in a similar manner to the natural
38 dose. For all three samples, the dose recovery ratios are in agreement with

1
2
3 unity within the error limits over the preheat temperature range of 200-260 °C
4 (Fig.2C). Based on these results a preheat temperature of 200 °C (for 10 s)
5 and a cut-heat temperature of 160 °C was identified as suitable for the
6 measurement of these samples (Table 2).
7
8

9
10 In order to verify the general suitability of the preheat and cut-heat
11 temperatures selected above, further dose-recovery tests were carried out on
12 all 29 samples (3-6 aliquots each). Fig. 3 presents a histogram of the
13 measured to given dose ratios. The average ratio was 1.009 ± 0.015 ($n = 135$)
14 for all the samples. However for some older samples especially these of which
15 the dose is larger than 120 Gy, the given dose cannot be recovered accurately.
16
17
18
19
20
21
22

23 *K-feldspar*

24
25 The greatest factor hampering the use of feldspars in luminescence dating is
26 the effect of anomalous fading of the luminescence signal (Wintle 1973).
27 Since the reporting of lower fading rates from post-IR IRSL (pIRIR) signals
28 measured at elevated temperature, compared to those from the conventional
29 IRSL measured at 50 °C (Thomsen *et al.* 2008), different pIRIR procedures
30 have been developed to minimize the effects of fading, including a two-step
31 (Buylaert *et al.* 2009; Thiel *et al.* 2011; Buylaert *et al.* 2012) and a multiple
32 elevated temperature (MET) post-IR IR stimulation procedure (Li & Li 2011,
33 2012). The robustness of ages based on pIRIR protocols without fading
34 correction has been confirmed by comparison with independent ages from
35 different sedimentary samples around the world (Buylaert *et al.* 2012; Arnold *et*
36 *al.* 2015). In our study, a series of measurements, including fading rate,
37 preheat plateau, dose recovery and bleachability tests under a wide range of
38 preheat and stimulation temperatures were carried out to investigate the
39 luminescence characteristics of pIRIR and IR₅₀ signals from sand-sized (63-90
40 µm) K-feldspar extracts. For these different tests, twenty-four aliquots were
41 prepared from samples 153001 and 153013. A preheat, varying from 180 to
42 320 °C with 20 °C increments, was given prior to the measurements of the
43 natural and regenerative dose as well as the test dose. The first IR stimulation
44
45
46
47
48
49
50
51
52
53
54
55
56
57
58
59
60

1
2
3 was carried out at 50 °C for 200 s (IR_{50}), followed by the second stimulation for
4 200 s with an elevated temperature (pIRIR) 30 °C below the preheat
5 temperature. At the end of the pIRIR response to each test dose, a 200 s ‘hot’
6 IR bleach at a temperature 5 °C higher than preheat temperature was used to
7 ensure a low residual of IRSL signal for the next cycle. The net IRSL signal
8 from K-feldspar was integrated from the first 1 s of stimulation minus the last
9 10 s as background. The detailed protocol is shown in Table 2.
10
11
12
13

14
15 Fig. 4 shows the IR_{50} and pIRIR₁₇₀ stimulation and dose response curves for
16 sample 153013. The IR_{50} signal intensity is higher than the pIRIR₁₇₀ signal.
17
18

19 Fig. 5 summarizes the equivalent dose, residual dose (after 4h bleaching in
20 solar simulator) and dose recovery ratio of IR_{50} and pIRIR signals as a function
21 of preheat temperature for samples 153001 and 153013. Fig. 5A shows the
22 mean D_e values obtained for the first IR_{50} stimulation with various preheat
23 temperatures. There is no systematic trend in D_e with the preheat temperature
24 used prior to the IR_{50} measurement, which is consistent with the observations
25 of Murray *et al.* (2009). This observation in HB loess also concurs with Alaskan
26 loess (Roberts 2012), and Qilian Shan loess (northeastern margin of TP)
27 (Zhang *et al.* 2015a). In contrast to the IR_{50} data, the pIRIR data indicate a
28 plateau up to ~220°C, beyond which there is a systematic increase in dose
29 with increasing preheat temperatures (from 280 to 320 °C) and stimulation
30 temperatures (from 250 to 290 °C) (Fig. 5B).
31
32
33
34
35
36
37
38

39 It is known that elevated-temperature IRSL bleaches more slowly than IRSL
40 stimulated at low temperatures (Poolton *et al.* 2002), and there may be a
41 residual component left even after a prolonged bleaching period (e.g. Kars *et*
42 *al.* 2014; Sohbati *et al.* 2016; Yi *et al.* 2016). The residual IR_{50} and pIRIR doses
43 plotted as a function of preheat temperature are shown in Fig. 5C and D,
44 respectively. For both IR_{50} and pIRIR signals, the residual doses gradually
45 increase with the preheat and stimulation temperatures, and larger residual
46 doses were obtained from the sample having larger D_e value (i.e. 153013), in
47 agreement with previous observations (e.g. Buylaert *et al.* 2012; Sohbati *et al.*
48 2012; Zhang *et al.* 2015b).
49
50
51
52
53
54
55

1
2
3 The IR₅₀ and pIRIR fading rates (g-values) of sample 153013 were
4 measured at different preheat temperatures, following Auclair *et al.* (2003) and
5 calculated after Huntley & Lamothe (2001) (Fig. 5 E, F). The IR₅₀ g-value
6 shows an apparent decreasing trend with increasing preheat temperature
7 varying from 2.9±0.3%/decade to 1.43±0.15%/decade, which is surprising in
8 view of the absence of any significant dependence of D_e on preheat
9 temperature. All pIRIR signals fade much less than the IR₅₀ signals; the
10 measured fading rates ranging between 0.84±0.16%/decade and
11 0.23±0.07%/decade and tend to decrease slightly with increasing preheat and
12 stimulation temperatures. The lower fading rate and thus higher signal stability
13 with increasing preheat/stimulation temperature is in line with the previous
14 observations (e.g. Jain & Ankjærgaard, 2011). All measured pIRIR fading rates
15 are less than 1%/decade; others have suggested that such low fading rates
16 may be laboratory artefacts (Thiel *et al.* 2011; Buylaert *et al.* 2012; Roberts
17 2012). In light of this, we have chosen not to fading correct for the observed
18 g-value.
19
20
21
22
23
24
25
26
27
28

29 For dose recovery tests, a laboratory beta dose equivalent to the average D_e
30 value of the natural preheat plateaus (i.e. ~40 Gy for 153001, and ~170 Gy for
31 153013) was added to aliquots which had been reset by 4 hours of light
32 exposure in a Hönle SOL2 solar simulator. Residual and added doses were
33 then measured as an 'unknown' dose using the same pIRIR protocol. The
34 recovered dose (Fig. 5G, H) was derived by subtracting the residual dose
35 following a 4h bleach (Fig. 5C, D) from the doses measured following
36 bleaching and dosing. For the IR₅₀ signals, the dose recovery ratio is
37 satisfactory over the preheat temperature range from 180 to 220 °C. For the
38 pIRIR signals, all of the dose recovery ratios except for 240 and 260 °C of
39 sample 153013 are within 10% of unity (Fig. 5H). Given the low residual dose
40 of pIRIR₁₇₀, the lower fading rate, and the excellent dose recovery ratio for both
41 IR₅₀ and pIRIR₁₇₀ at preheat temperature of 200 °C, a SAR protocol using
42 pIRIR₁₇₀ was employed to date the HB loess section. The pIRIR₁₇₀ signal used
43 in this study is generally similar in behaviour to that from a loess section in Arid
44 Central Asia described by Li *et al.* (2015); they also describe a low residual
45
46
47
48
49
50
51
52
53
54
55

1
2
3 dose (<1.3 Gy) and low fading rate (~1%/dec.). Here, we measured 12–15
4 cups for each sample to give the mean D_e (and associated standard error).
5
6
7

8 9 *Bleaching characteristics*

10
11 The completeness of the bleaching of quartz can be determined based on the
12 differential bleaching rates of quartz and feldspar luminescence signals
13 (Murray *et al.* 2012). The quartz OSL signal decreases much more rapidly than
14 the IR₅₀ and pIRIR signals during broadband stimulation; after ~30 s bleaching
15 the quartz OSL in sample 153003 has been reduced to ~5% of its original level,
16 while the feldspar IR₅₀ and pIRIR₁₇₀ signals are still at ~24 and ~65%,
17 respectively (Fig. 6A). It takes ~240 s to reduce the IR₅₀ signal to a negligible
18 level (~3.8%), while it takes 7200 s to reduce pIRIR₁₇₀ signal to a similar level
19 (~5%, Fig. 6A). Fig. 6C shows the very strong correlation between D_e values
20 based on IR₅₀ and pIRIR₁₇₀ over the entire dose range. Either all samples have
21 been incompletely-bleached to the same degree or, more likely, all samples
22 have been completely bleached (see also Sohbaty *et al.* 2016).
23
24
25
26
27
28
29
30
31

32 The dependence of both IR₅₀ and pIRIR₁₇₀ residual doses on solar bleaching
33 time was also investigated. Nine sets of aliquots from sample 153003 were
34 bleached under the solar simulator for various times from 1h to 256h; the
35 residual doses were then measured using the same pIRIR₁₇₀ protocol. The
36 bleaching rate of IR₅₀ and pIRIR₁₇₀ decreases with stimulation time (Fig. 6B).
37 For the IR₅₀ signal, the residual dose is reduced to 1.04 ± 0.03 Gy, ~1.3% of
38 the natural dose of 76 Gy, after only 1 h of SOL2 exposure; it then continues to
39 decrease slowly. For the pIRIR₁₇₀ signal, the residual dose is reduced
40 relatively quickly over the first 4 h of bleaching, decreasing from a natural dose
41 of 97 to 4.3 Gy i.e. <5% of the natural dose. After 4 h bleaching, the dose
42 recorded by the pIRIR₁₇₀ signal continues to decrease slowly. Both the IR₅₀
43 and pIRIR₁₇₀ signals are still decreasing after 11 days of solar stimulator
44 exposure (see also Kars *et al.* 2014). Given these observations, and the
45 absence of any significant intercept in Fig. 6C, no residual dose was
46 subtracted in any of our age calculations; this is a conservative calculation
47
48
49
50
51
52
53
54
55
56

1
2
3 since the main use of the feldspar ages is to confirm the degree of bleaching of
4 the quartz at deposition.
5
6
7
8

9 **HB loess age**

10
11
12 Quartz OSL and K-feldspar IR₅₀ and pIRIR₁₇₀ equivalent doses and ages
13 are summarized in Table 3. Fig. 7A summarizes the comparison between OSL
14 and fading-corrected IR₅₀ ages. For the IR₅₀ ages, the *g*-value of ~2.6%/dec.
15 measured from the sample 153013 was applied to all samples, and the
16 correction follows Huntley & Lamothe (2001). Note that following the
17 observations of Buylaert *et al.* (2011) and Singh *et al.* (2017), we do not
18 attempt to apply aliquot- or sample-specific fading rates. As expected,
19 uncorrected IR₅₀ ages underestimate those from quartz. After application of
20 the fading correction, the IR₅₀ ages tend to overestimate those from quartz
21 especially at higher doses (equivalent to >40 ka). On the other hand, pIRIR₁₇₀
22 and quartz ages show good agreement for samples whose quartz age is <40
23 ka (Fig. 7B); for samples with quartz ages >40 ka (i.e. $D_e > 120$ Gy) the
24 pIRIR₁₇₀ ages tend to be older than quartz ages. This is not surprising as it has
25 often been reported that quartz tends to underestimate age for doses greater
26 than ~150 Gy (e.g. Chapot *et al.* 2012; Timar-Gabor & Wintle 2013). As a
27 result, we restrict our use of quartz ages to $D_e < 120$ Gy; this observation is
28 consistent with previous work on the western Chinese loess plateau (e.g.
29 Buylaert *et al.* 2007; Buylaert *et al.* 2008) and Tianshan Mountains, arid central
30 Asia (e.g. Li *et al.* 2016).
31
32
33
34
35
36
37
38
39
40
41
42
43

44 The corrected IR₅₀ and pIRIR₁₇₀ ages from these samples are similar to one
45 another; since the IR₅₀ signal bleaches more rapidly than pIRIR signals (e.g.
46 Colarossi *et al.* 2015), this probably indicates that both feldspar signals are
47 fully bleached. However, the quartz ages from the upper two samples with
48 depth of 10 and 40 cm are significantly younger than the feldspar ages. This
49 suggests a very short, recent bleaching event, sufficient to reset quartz OSL,
50 at least partially, but not sufficient to significantly affect feldspar signals. This
51
52
53
54
55
56
57
58
59
60

1
2
3 would be consistent with agricultural disturbance, and in turn suggests that
4 these two quartz ages cannot be used as reliable indicators of primary
5 deposition time. On the other hand, the feldspar ages from these samples
6 probably do give a more accurate indication of primary deposition, and suggest
7 a minimum age of the loess deposit of 10.8 ± 0.5 ka.
8
9
10

11 Finally, two radiocarbon ages obtained from the well-preserved snails at
12 depths of 615 and 725 cm are 40.1 ± 0.6 ka BP (42.8–44.8 cal. ka BP) and
13 39.8 ± 0.4 ka BP (42.8–44.2 cal. ka BP), respectively. Both these ages are
14 approaching the practical age limit for ^{14}C . Because of the dose rate, this age
15 range happens to be in the same dose range at which quartz begins to
16 systematically underestimate (see above). Thus the apparent agreement
17 between ^{14}C and quartz ages in the deeper samples is probably coincidental;
18 both are likely underestimates. At this stage in our work, we assume that the
19 older feldspar ages at this depth and below is more likely to be correct. This
20 conclusion is consistent with those of previous studies in Xinjiang mountain
21 loess, western China (E *et al.* 2012; Song *et al.* 2015).
22
23
24
25
26
27
28
29

30 Given that the consistency between quartz and feldspar age for samples
31 younger than 40 ka, and the known underestimate of quartz in loess >40 ka,
32 the average quartz OSL and pIRIR₁₇₀ feldspar ages were taken to represent
33 the aeolian loess deposition ages up to 40 ka and the feldspar ages alone
34 used beyond that. The ages of sample 153005 and 153006 are obviously
35 outliers, and these two ages have been excluded from further analysis. The
36 final accepted ages are plotted as a function of depth in Fig. 8A together with
37 the ^{14}C ages. An age-depth model derived using the Bacon code (Blaauw &
38 Christen 2011) is also shown (solid blue line) fitted to the accepted
39 luminescence ages from 40 cm and below; 65% confidence intervals are
40 shown as solid green lines. Finally, mass accumulation rates (MAR) are
41 derived from the modelled fit (Fig. 8B), assuming a loess density of 1.50 g cm^{-3}
42 (Kohfeld & Harrison 2003; Buylaert *et al.* 2015).
43
44
45
46
47
48
49
50
51

52 Discussion

53
54
55
56
57
58
59
60

1
2
3 The HB loess section appears to record continuous environmental information
4 from ~50 to ~30 ka, i.e. throughout the relatively warm and humid Marine
5 Isotope Stage (MIS) 3 (Voelker 2002). There was considerable variation in
6 MAR during MIS 3 at the HB section. Dust accumulation was relatively
7 constant at $\sim 350 \text{ g m}^{-2} \text{ a}^{-1}$ between ~50 and ~40 ka, but then rapidly doubled at
8 ~38 ka. MAR then decreased to the earlier level, with a minimum rate at ~33
9 ka before increasing again after ~32 ka (Fig. 8B). We first compare our record
10 with Huangshuiping loess section at the margin of northeast TP (located in
11 Fig.1B) and then with a central CLP site. The similar rapid dust deposition
12 event around 30-33 ka was recorded in the Hongshuiping loess section (Wang
13 *et al.* 2015). The flux of $>25 \mu\text{m}$ fraction grains (considered as an indicator of
14 the aeolian contribution) to the lake sediments in Qinghai lake also suggests a
15 rapid accumulation rate between 32 and 29 ka (An *et al.* 2012). Both studies
16 are in line with our high MAR value at ~32 ka. The relatively low and stable
17 dust accumulation rate between ~50 and ~40 ka at our site (Fig. 8B) may
18 indicate a relatively weak dust source during early MIS 3, perhaps because of
19 increased vegetation cover, a mechanism suggested by Ujvari *et al.* (2017) for
20 European loess. Comparison between our MAR data and those of Stevens *et*
21 *al.* (2016) from the central CLP (Xifeng site; Fig. S1) shows a similar MAR
22 pattern for MIS 3. However, the Xifeng data indicate much lower MAR values
23 (~25% of HB) although the relative change from low to high MAR values is
24 similar (approximately double).
25
26
27
28
29
30
31
32
33
34
35
36
37
38

39 In contrast to the continuous MIS 3 record, almost all of MIS 1 and the entire
40 MIS 2 are missing at Hebei (Fig. 8) – even the presence of sediment from MIS
41 1 at this site is demonstrated only by a sample that was probably exposed to
42 light after primary deposition. The lack of MIS 1 dates is in contrast to previous
43 work, which suggests that in most regions of the TP the most rapid loess
44 accumulation occurred during the Lateglacial and in the early Holocene (based
45 on 353 OSL ages from in total 109 individual sections, Stauch 2015).
46 Furthermore, in our study area, the basal age of the Holocene SHD loess
47 section, ~80 km south of our HB section, is $10.7 \pm 1 \text{ ka}$ (Lehmkuhl *et al.* 2014),
48 and two OSL dates on two till sections of loess composition near the
49
50
51
52
53
54
55

1
2
3 Anyemaqen Mountains are 12.3 ± 1.1 and 7.1 ± 0.7 ka (Owen *et al.* 2003).
4 Combined with the top sample age of 10.8 ± 0.5 ka in the HB section, these
5 published dates indicate that deposition of loess continued during the
6 Holocene and the Lateglacial (Owen *et al.* 2003; Lehmkuhl *et al.* 2014).
7
8
9

10 However, there are almost no published loess dates from the TP that fall
11 during the Last Glacial Maximum (LGM, from ~ 26 to ~ 19 ka ago). For instance,
12 Buylaert *et al.* (2008) identified an important hiatus between ~ 20 and ~ 30 ka at
13 the Tuxiangdao site on the margin of the northeast TP. In addition, low dust
14 accumulation rates (< 5 cm ka⁻¹ for TX loess section and ~ 10 cm ka⁻¹ for ML
15 loess section) can be calculated from the published data for the ML and TX
16 loess sections in the Gonghe basin during the LGM (Qiang *et al.* 2016),
17 although this is based on a limited number of ages. In our view an erosional
18 hiatus in these sequences is a more likely explanation, similar to that found in
19 our HB section (Fig. 8A); the alternative of prolonged low accumulation rates
20 seems less likely in such a dynamic intramontane basin. Fig. 9 summarizes
21 the distribution of loess-palaeosol luminescence ages in the northeast TP
22 (based on our data and data from Küster *et al.* 2006; Lu *et al.* 2011; Liu *et al.*
23 2012; Stauch *et al.* 2012; Liu *et al.* 2013; Qiang *et al.* 2013; Lehmkuhl *et al.*
24 2014; Yu & Lai 2014; Liu *et al.* 2015; Zhang *et al.* 2015a; Qiang *et al.* 2016; Liu
25 *et al.* 2017). It can be seen that loess deposition in Tibet is predominantly an
26 interglacial/interstadial phenomenon. However it must be recognized that,
27 except for the HB section, the other sections were sampled at a relatively low
28 spatial (depth) resolution, and more high resolution chronological studies are
29 required to confirm this hypothesis.
30
31
32
33
34
35
36
37
38
39
40
41
42

43 In contrast, dust deposition and high MAR values in the CLP seem to occur
44 mainly during glacial periods (e.g. Kang *et al.* 2015) suggesting that the TP
45 may be deflating at the same time as the CLP is accumulating, at least during
46 MIS 2. The obvious inference that the TP provides at least part of the source of
47 CLP loess is consistent with the conclusions of recent provenance studies
48 (Bird *et al.* 2015; Nie *et al.* 2015; Fenn *et al.* 2017).
49
50
51
52
53
54
55

Conclusions

A high sampling resolution chronological study was carried out at the HB loess section on east-facing slopes of the Anyemaqen Mountains in the northeast TP. Both quartz OSL and feldspar IRSL signals were used to derive ages. Quartz OSL and feldspar pIRIR₁₇₀ ages are in good agreement back to ~40 ka (corresponding quartz D_e ~120 Gy). Beyond this, feldspar pIRIR₁₇₀ ages are considered more reliable. The agreement between quartz and feldspar ages up to ~40 ka confirms that both signals are sufficiently well bleached in this age range, and so it is reasonable to conclude that older feldspar samples were also well bleached. We deduce that quartz D_e values obtained from the SAR protocol used here with sand-sized (63-90 μm) grains should not be considered reliable above ~120 Gy. The HB loess section records continuous environmental information of the entire MIS 3 period (50-30 ka). Calculated mass accumulation rates (MAR) varied considerably over this period. During early MIS 3 (50-40 ka) dust accumulation was relatively low and stable but then rapidly increased to peak at ~38 ka. MAR values then decreased to reach a low at ~33 ka; after ~32 ka MAR values almost doubled within a few ka. Our results also suggest an erosional hiatus during MIS 2 which is in line with the absence of MIS 2 loess ages on the TP. We suggest that loess deposition on the Tibetan Plateau is predominantly an interglacial/interstadial phenomenon but more high resolution chronological studies, especially in the central TP, are required to fully test this hypothesis.

Acknowledgements.- This study was supported by a China NSF grant (41761042), NSF grant of Qinghai Province (2017-ZJ-901), and CAS "Light of West China" Program (2018-3-10). Alastair Cunningham is thanked for help with the Kernel density plot. Thomas Stevens is thanked for useful discussions. We thank the anonymous reviewers for providing valuable comments on the manuscript and Li Fan for his help in the field.

References

- An, Z., Colman, S. M., Zhou, W., Li, X., Brown, E. T., Jull, A. T., Cai, Y., Huang, Y., Lu, X. & Chang, H. 2012: Interplay between the Westerlies and Asian monsoon recorded in Lake Qinghai sediments since 32 ka. *Scientific Reports* 2, 1-7.
- An, Z., Kukla, G., Porter, S. C. & Xiao, J. 1991: Late quaternary dust flow on the Chinese Loess Plateau. *Catena* 18, 125-132.
- Arnold, L.J., Demuro, M., Parés, J.M., Pérez-González, A., Arsuaga, J.L., Bermúdez de Castro, J.M. & Carbonell, E., 2015: Evaluating the suitability of extended-range luminescence dating techniques over early and Middle Pleistocene timescales: Published datasets and case studies from Atapuerca, Spain. *Quaternary International* 389, 167-190.
- Ballarini, M., Wallinga, J., Wintle, A. G. & Bos, A. J. J. 2007: A modified SAR protocol for optical dating of individual grains from young quartz samples. *Radiation Measurements* 42, 360-369.
- Blaauw, M. & Christen, J. A. 2011: Flexible paleoclimate age-depth models using an autoregressive gamma process. *Bayesian Analysis* 6, 457-474.
- Bøtter-Jensen, L., Thomsen, K. J. & Jain, M. 2010: Review of optically stimulated luminescence (OSL) instrumental developments for retrospective dosimetry. *Radiation Measurements* 45, 253-257.
- Bird, A., Stevens, T., Rittner, M., Vermeesch, P., Carter, A., Andò, S., Garzanti, E., Lu, H., Nie, J., Zeng, L., Zhang, H. & Xu, Z. 2015: Quaternary dust source variation across the Chinese Loess Plateau. *Palaeogeography, Palaeoclimatology, Palaeoecology* 435, 254-264.
- Buylaert, J.-P., Yeo, E.-Y., Thiel, C., Yi, S., Stevens, T., Thompson, W., Frechen, M., Murray, A., Lu, H., 2015: A detailed post-IR IRSL chronology for the last interglacial soil at the Jingbian loess site (northern China). *Quaternary Geochronology* 30, 194-199.
- Buylaert, J.-P., Jain, M., Murray, A. S., Thomsen, K. J., Thiel, C. & Sohbati, R. 2012: A robust feldspar luminescence dating method for Middle and Late Pleistocene sediments. *Boreas* 41, 435-451.
- Buylaert, J.-P., Murray, A., Vandenberghe, D., Vriend, M. & De Corte, F. 2008: Optical dating of Chinese loess using sand-sized quartz: Establishing a time frame for Late Pleistocene climate changes in the western part of the Chinese Loess Plateau. *Quaternary Geochronology* 3, 99-113.
- Buylaert, J. P., Murray, A. S., Thomsen, K. J. & Jain, M. 2009: Testing the potential of an elevated temperature IRSL signal from K-feldspar. *Radiation Measurements* 44, 560-565.
- Buylaert, J. P., Vandenberghe, D., Murray, A. S., Huot, S., De Corte, F. & Van den Haute, P. 2007: Luminescence dating of old (>70 ka) Chinese loess: A comparison of single-aliquot OSL and IRSL techniques. *Quaternary Geochronology* 2, 9-14.
- Chapot, M. S., Roberts, H. M., Duller, G. A. T. & Lai, Z. P. 2012: A comparison of natural- and laboratory-generated dose response curves for quartz optically stimulated luminescence signals from Chinese Loess. *Radiation Measurements* 47, 1045-105.
- Cunningham, A. C. & Wallinga, J. 2010: Selection of integration time intervals for quartz OSL decay curves. *Quaternary Geochronology* 5, 657-666.
- Daut, G., Mäusbacher, R., Baade, J., Gleixner, G., Kroemer, E., Mügler, I., Wallner, J., Wang, J. & Zhu, L. 2010: Late Quaternary hydrological changes inferred from

- lake level fluctuations of Nam Co (Tibetan Plateau, China). *Quaternary International* 218, 86-93.
- Duller, G. A. T. 2003: Distinguishing quartz and feldspar in single grain luminescence measurements. *Radiation Measurements* 37, 161-165.
- E, C., Lai, Z., Sun, Y., Hou, G., Yu, L. & Wu, C. 2012: A luminescence dating study of loess deposits from the Yili River basin in western China. *Quaternary Geochronology* 10, 50-55.
- Fang, X., Chen, F., Shi, Y. & Li, J. 1996: Garze loess and the evolution of the cryosphere on the Tibetan Plateau. *Journal of Glaciology and Geocryology* 18, 193-200 (in Chinese).
- Fenn, K., Stevens, T., Bird, A., Limonta, M., Rittner, M., Vermeesch, P., Andò, S., Garzanti, E., Lu, H., Zhang, H. & Lin, Z. 2017: Insights into the provenance of the Chinese Loess Plateau from joint zircon U-Pb and garnet geochemical analysis of last glacial loess. *Quaternary Research*, Doi:10.1017/qua.2017.86
- Guérin, G., Mercier, N., Nathan, R., Adamiec, G. & Lefrais, Y. 2012: On the use of the infinite matrix assumption and associated concepts: A critical review. *Radiation Measurements* 47, 778-785.
- Hansen, V., Murray, A., Buylaert, J.-P., Yeo, E.-Y. & Thomsen, K. 2015: A new irradiated quartz for beta source calibration. *Radiation Measurements* 81, 123-127.
- Huntley, D. J. & Baril, M. R. 1997: The K content of the K-feldspars being measured in optical dating or in thermoluminescence dating. *Ancient TL* 15, 11-13.
- Huntley, D. J. & Lamothe, M. 2001: Ubiquity of anomalous fading in K-feldspars and the measurement and correction for it in optical dating. *Canadian Journal of Earth Sciences* 38, 1093-1106.
- Huntley, D.J. & Hancock, R.G.V. 2001: The Rb contents of the K-feldspar grains being measured in optical dating. *Ancient TL* 19, 43-46.
- Jain, M. & Ankjærgaard, C., 2011: Towards a non-fading signal in feldspar: Insight into charge transport and tunnelling from time-resolved optically stimulated luminescence. *Radiation Measurement* 46, 292-309.
- Kaiser, K., Lai, Z., Schneider, B. & Junge, F. W. 2010: Late Pleistocene genesis of the middle Yarlung Zhangbo Valley, southern Tibet (China), as deduced by sedimentological and luminescence data. *Quaternary Geochronology* 5, 200-204.
- Kang, S. G., Roberts, H. M., Wang, X. L., An, Z. S. & Wang, M. 2015: Mass accumulation rate changes in Chinese loess during MIS 2, and asynchrony with records from Greenland ice cores and North Pacific Ocean sediments during the Last Glacial Maximum. *Aeolian Research* 19, 251-258.
- Kars, R. H., Reimann, T., Ankjærgaard, C. & Wallinga, J. 2014: Bleaching of the post-IR IRSL signal: new insights for feldspar luminescence dating. *Boreas* 43, 780-791.
- Kohfeld K.E. & Harrison, S.P. 2003: Glacial-interglacial changes in dust deposition on the Chinese Loess Plateau. *Quaternary Science Reviews* 22, 1859-1878.
- Küster, Y., Hetzel, R., Krbetschek, M. & Tao, M.X. 2006: Holocene loess sedimentation along the Qilian Shan (China): significance for understanding the processes and timing of loess deposition. *Quaternary Science Reviews* 25, 114-125.
- Lai, Z., Kaiser, K. & Brückner, H. 2009: Luminescence-dated aeolian deposits of late Quaternary age in the southern Tibetan Plateau and their implications for landscape history. *Quaternary Research* 72, 421-430.

- 1
2
3 Lehmkuhl, F., Klinge, M., Rees-Jones, J. & Rhodes, E. J. 2000: Late Quaternary aeolian
4 sedimentation in central and south-eastern Tibet. *Quaternary International*
5 *68–71*, 117-132.
- 6 Lehmkuhl, F., Schulte, P., Zhao, H., Hülle, D., Protze, J. & Stauch, G. 2014: Timing and
7 spatial distribution of loess and loess-like sediments in the mountain areas of
8 the northeastern Tibetan Plateau. *Catena* *117*, 23-33.
- 9 Li, B. & Li, S.-H. 2006: Comparison of estimates using the fast component and the
10 medium component of quartz OSL. *Radiation Measurements* *41*, 125-136.
- 11 Li, B. & Li, S.-H. 2011: Luminescence dating of K-feldspar from sediments: A protocol
12 without anomalous fading correction. *Quaternary Geochronology* *6*, 468-479.
- 13 Li, B. & Li, S.-H. 2012: Luminescence dating of Chinese loess beyond 130 ka using the
14 non-fading signal from K-feldspar. *Quaternary Geochronology* *10*, 24-31.
- 15 Li, G., Wen, L., Xia, D., Duan, Y., Rao, Z., Madsen, D. B., Wei, H., Li, F., Jia, J. & Chen,
16 F. 2015: Quartz OSL and K-feldspar pIRIR dating of a loess/paleosol sequence
17 from arid central Asia, Tianshan Mountains, NW China. *Quaternary*
18 *Geochronology* *28*, 40-53.
- 19 Li, G., Rao, Z., Duan, Y., Xia, D., Wang, L., Madsen, D. B., Jia, J., Wei, H., Qiang, M.,
20 Chen, J. & Chen, F. 2016: Paleoenvironmental changes recorded in a
21 luminescence dated loess/paleosol sequence from the Tianshan Mountains, arid
22 central Asia, since the Penultimate Glaciation. *Earth and Planetary Science Letters*
23 *448*, 1-12.
- 24 Liu, B., Jin, H., Sun, L., Sun, Z., Su, Z., & Zhang, C 2013: Holocene climatic change
25 revealed by aeolian deposits from the gonghe basin, northeastern
26 qinghai–tibetan plateau. *Quaternary International* *296*, 231-240.
- 27 Liu, X.-J., Xiao, G., E, C., Li, X., Lai, Z., Yu, L. & Wang, Z. 2017: Accumulation and
28 erosion of aeolian sediments in the northeastern Qinghai-Tibetan Plateau and
29 implications for provenance to the Chinese Loess Plateau. *Journal of Asian*
30 *Earth Sciences* *135*, 166-174.
- 31 Liu, X., Lai, Z., Yu, L., Sun, Y. & Madsen, D. 2012: Luminescence chronology of aeolian
32 deposits from the Qinghai Lake area in the Northeastern Qinghai-Tibetan
33 Plateau and its palaeoenvironmental implications. *Quaternary Geochronology*
34 *10*, 7-43.
- 35 Lu, H., Wang, X. & Sun X. 2007: Loess stratigraphy and palaeoclimate changes during
36 Quaternary in North Eastern Tibetan Plateau revealed by loess core.
37 *Quaternary Sciences* *27*, 230-241.
- 38 Lu, H., Wang, X., Ma, H., Tan, H., Vandenberghe, J., Miao, X., Li, Z., Sun, Y., An, Z. &
39 Cao, G. 2004: The Plateau Monsoon variation during the past 130 kyr revealed
40 by loess deposit at northeast Qinghai–Tibet (China). *Global and Planetary*
41 *Change* *41*, 207-214.
- 42 Lu, H., Zhao, C., Mason, J., Yi, S., Zhao, H., Zhou, Y., Ji, J., Swinehart, J. & Wang, C.
43 2011: Holocene climatic changes revealed by aeolian deposits from the Qinghai
44 Lake area (northeastern Qinghai-Tibetan Plateau) and possible forcing
45 mechanisms. *The Holocene* *21*, 297-304.
- 46 Mejdahl, V. 1987: Internal radioactivity in quartz and feldspar grains. *Ancient TL* *5*,
47 10-17.
- 48 Mischke, S., Zhang, C., Börner, A. & Herzsuh, U. 2010: Lateglacial and Holocene
49 variation in aeolian sediment flux over the northeastern Tibetan Plateau
50 recorded by laminated sediments of a saline meromictic lake. *Journal of*
51 *Quaternary Science* *25*, 162–177.
- 52 Murray, A. S., Buylaert, J. P., Thomsen, K. J. & Jain, M. 2009: The effect of preheating
53 on the IRSL signal from feldspar. *Radiation Measurements* *44*, 554-559.

- 1
2
3 Murray, A. S., Marten, R., Johnston, A. & Martin, P. 1987: Analysis for naturally
4 occurring radionuclides at environmental concentrations by gamma
5 spectrometry. *Journal of Radioanalytical and Nuclear Chemistry* 115, 263-288.
- 6 Murray, A. S., Thomsen, K. J., Masuda, N., Buylaert, J. P. & Jain, M. 2012: Identifying
7 well-bleached quartz using the different bleaching rates of quartz and feldspar
8 luminescence signals. *Radiation Measurements* 47, 688-695.
- 9 Murray, A. S. & Wintle, A. G. 2000: Luminescence dating of quartz using an improved
10 single-aliquot regenerative-dose protocol. *Radiation Measurements* 32, 57-73.
- 11 Murray, A. S. & Wintle, A. G. 2003: The single aliquot regenerative dose protocol:
12 potential for improvements in reliability. *Radiation Measurements* 37, 377-381.
- 13 Nie, J., Stevens, T., Rittner, M., Stockli, D., Garzanti, E., Limonta, M., Bird, A., Andò,
14 S., Vermeesch, P., Saylor, J., Lu, H., Breecker, D., Hu, X., Liu, S., Resentini, A.,
15 Vezzoli, G., Peng, W., Carter, A., Ji, S. & Pan, B. 2015: Loess plateau storage of
16 northeastern Tibetan plateau-derived yellow river sediment. *Nature*
17 *Communications* 6, 8511. DOI: 10.1038/ncomms9511.
- 18 Owen, L. A., Finkel, R. C., Haizhou, M. & Barnard, P. L. 2006: Late Quaternary
19 landscape evolution in the Kunlun Mountains and Qaidam Basin, Northern
20 Tibet: A framework for examining the links between glaciation, lake level
21 changes and alluvial fan formation. *Quaternary International* 154-155, 73-86.
- 22 Owen, L. A., Finkel, R. C., Haizhou, M., Spencer, J. Q., Derbyshire, E., Barnard, P. L. &
23 Caffee, M. W. 2003: Timing and style of Late Quaternary glaciation in
24 northeastern Tibet. *Geological Society of America Bulletin* 115, 1356-1364.
- 25 Pigati, J.S., Quade, J., Wilson, J., Jull, A.J.T., & Lifton, N.A., 2007: Development of
26 lowbackground vacuum extraction and graphitization systems for 14C dating of
27 old (40-60 ka) samples. *Quaternary International* 166, 4-14.
- 28 Poolton, N. R. J., Ozanyan, K. B., Wallinga, J., Murray, A. S. & Bøtter-Jensen, L. 2002:
29 Electrons in feldspar II: a consideration of the influence of conduction band-tail
30 states on luminescence processes. *Physics and Chemistry of Minerals* 29,
31 217-225.
- 32 Prescott, J. R. & Hutton, J. T. 1994: Cosmic ray contributions to dose rates for
33 luminescence and ESR dating: Large depths and long-term time variations.
34 *Radiation Measurements* 23, 497-500.
- 35 Qiang, M., Chen, F., Song, L., Liu, X., Li, M. & Wang, Q. 2013: Late Quaternary aeolian
36 activity in Gonghe Basin, northeastern Qinghai-Tibetan Plateau, China.
37 *Quaternary Research* 79, 403-412.
- 38 Qiang, M., Jin, Y., Liu, X., Song, L., Li, H., Li, F. & Chen, F. 2016: Late Pleistocene and
39 Holocene aeolian sedimentation in Gonghe Basin, northeastern
40 Qinghai-Tibetan Plateau: Variability, processes, and climatic implications.
41 *Quaternary Science Reviews* 132, 57-73.
- 42 Qiu, J. 2008: China: the third pole. *Nature News* 454, 393-396.
- 43 Roberts, H. M. 2012: Testing Post-IR IRSL protocols for minimising fading in feldspars,
44 using Alaskan loess with independent chronological control. *Radiation*
45 *Measurements* 47, 716-724.
- 46 Singh, A., Thomsen, K.J., Sinha, R., Buylaert, J.-P., Carter, A., Mark, D.F., Mason, P.J.,
47 Densmore, A.L., Murray, A.S., Jain, M., Paul, D. & Gupta, S. 2017:
48 Counter-intuitive influence of Himalayan river morphodynamics on Indus
49 Civilisation urban settlements. *Nature Communications* 8, 1617.
50 DOI: 10.1038/s41467-017-01643-9.
- 51 Sohbaty, R., Murray, A. S., Buylaert, J.-P., Ortuño, M., Cunha, P. P. & Masana, E. 2012:
52 Luminescence dating of Pleistocene alluvial sediments affected by the Alhama
53
54
55

- de Murcia fault (eastern Betics, Spain) – a comparison between OSL, IRSL and post-IRIRSL ages. *Boreas* 41, 250-262.
- Sohbati, R., Borella, J., Murray, A., Quigley, M. & Buylaert, J.P. 2016: Optical dating of loessic hillslope sediments constrains timing of prehistoric rockfalls, Christchurch, New Zealand. *Journal of Quaternary Science* 31, 678–690.
- Stauch, G. 2015: Geomorphological and palaeoclimate dynamics recorded by the formation of aeolian archives on the Tibetan Plateau. *Earth-Science Reviews* 150, 393-408.
- Stauch, G., Ijmker, J., Pötsch, S., Zhao, H., Hilgers, A., Diekmann, B., Dietze, E., Hartmann, K., Opitz, S. & Wünnemann, B. 2012: Aeolian sediments on the north-eastern Tibetan Plateau. *Quaternary Science Reviews* 57, 71-84.
- Sun, J., Li, S.-H., Muhs, D. R. & Li, B. 2007: Loess sedimentation in Tibet: provenance, processes, and link with Quaternary glaciations. *Quaternary Science Reviews* 26, 2265-2280.
- Thiel, C., Buylaert, J.-P., Murray, A., Terhorst, B., Hofer, I., Tsukamoto, S. & Frechen, M. 2011: Luminescence dating of the Stratzing loess profile (Austria) – Testing the potential of an elevated temperature post-IR IRSL protocol. *Quaternary International* 234, 23-31.
- Timar-Gabor, A. & Wintle, A. G. 2013: On natural and laboratory generated dose response curves for quartz of different grain sizes from Romanian loess. *Quaternary Geochronology* 18, 34-40.
- Thomsen, K. J., Murray, A. S., Jain, M. & Bøtter-Jensen, L. 2008: Laboratory fading rates of various luminescence signals from feldspar-rich sediment extracts. *Radiation Measurements* 43, 1474-1486.
- Thrasher, I. M., Mauz, B., Chiverrell, R. C. & Lang, A. 2009: Luminescence dating of glaciofluvial deposits: A review. *Earth-Science Reviews* 97, 133-146.
- Újvári, G., Stevens, T., Molnár, M., Demény, A., Lambert, F., Varga, G., Timothy Jull, A. J., Páll-Gergely, B., Buylaert, J.-P. & Kovács, J. 2017: Coupled European and Greenland last glacial dust activity driven by North Atlantic climate. *Proceedings of the National Academy of Sciences* 114, E10632-E10638.
- Voelker, A. H. L. 2002: Global distribution of centennial-scale records for Marine Isotope Stage (MIS) 3: a database. *Quaternary Science Reviews* 21, 1185-1212.
- Wang, X., Yi, S., Lu, H., Vandenberghe, J. & Han, Z. 2015: Aeolian process and climatic changes in loess records from the northeastern Tibetan Plateau: Response to global temperature forcing since 30 ka. *Paleoceanography* 30, 612-620.
- Wintle, A. G. 1973: Anomalous fading of thermo-luminescence in mineral samples. *Nature* 245, 143-144.
- Wintle, A. G. & Murray, A. S. 2006: A review of quartz optically stimulated luminescence characteristics and their relevance in single-aliquot regeneration dating protocols. *Radiation Measurements* 41, 369-391.
- Yang, S., Fang, X., Shi, Z., Lehmkuhl, F., Song, C., Han, Y. & Han, W. 2010: Timing and provenance of loess in the Sichuan Basin, southwestern China. *Palaeogeography, Palaeoclimatology, Palaeoecology* 292, 144-154.
- Yi, S., Buylaert, J.P., Murray, A.S., Lu, H., Thiel, C. & Zeng, L. 2016: A detailed post-IR IRSL dating study of the Niuyangzigou loess site in northeastern China. *Boreas* 45, 644–657.
- Yu, L. & Lai, Z. 2014: Holocene climate change inferred from stratigraphy and OSL chronology of aeolian sediments in the Qaidam Basin, northeastern Qinghai–Tibetan Plateau. *Quaternary Research* 81, 488-499.

- 1
2
3 Zhang, J., Nottebaum, V., Tsukamoto, S., Lehmkuhl, F. & Frechen, M. 2015a: Late
4 Pleistocene and Holocene loess sedimentation in central and western Qilian
5 Shan (China) revealed by OSL dating. *Quaternary International* 372, 120-129.
6 Zhang, J., Tsukamoto, S., Nottebaum, V., Lehmkuhl, F. & Frechen, M. 2015b: De
7 plateau and its implications for post-IR IRSL dating of polymineral fine grains.
8 *Quaternary Geochronology* 30, 147-153.
9 Zhao, H. & Li, S.-H. 2005: Internal dose rate to K-feldspar grains from radioactive
10 elements other than potassium. *Radiation Measurements* 40, 84-93.
11
12
13
14
15
16
17
18
19
20
21
22
23
24
25
26
27
28
29
30
31
32
33
34
35
36
37
38
39
40
41
42
43
44
45
46
47
48
49
50
51
52
53
54
55
56
57
58
59
60

For Review Only

Captions

Fig. 1. A. An overview of the study area in the Tibetan Plateau, China. B. The location of the HB (Hebei) loess section and the previously published loess sections nearby HB including Suohuduo (SHD) (Lehmkuhl *et al.* 2014), the T21 and T27 loess sections in Anyemaqen mountains (Owen *et al.* 2003), Mangla (ML) and Taxiu (TX) loess sections in Gonghe Basin (Qiang *et al.* 2016), and Hongshuiping (HS) loess section (Wang *et al.* 2015) and Tuxiangdao (TXD) loess section (Buylaert *et al.* 2008) in western loess plateau.

Fig. 2. Sand-sized (63-90 μm) quartz grain luminescence characteristics. A. Dose-response curve for sample 153001 (inset shows the natural stimulation curve). B. Preheat plateau tests of three samples from the top (153001), middle (153013) and bottom (153029) of the section. The dashed lines represents the average D_e over the 160-280 $^{\circ}\text{C}$ interval for sample 153001, and over the 160-240 $^{\circ}\text{C}$ interval for samples 153013 and 153029. C. Dose recovery preheat plateau tests of the same samples as in (B) Three aliquots were measured at each temperature. Error bars represent one standard error. There are no data points for sample 153001 at 280 and 300 $^{\circ}\text{C}$ in (B) and (C) and for sample 153029 at 300 $^{\circ}\text{C}$ in (B) due to the absence of signal after preheating to these temperatures.

Fig. 3. The distribution of dose recovery ratios for quartz. All samples were measured under the preheat temperature of 200 $^{\circ}\text{C}$ and cutheat temperature of 160 $^{\circ}\text{C}$.

Fig. 4. Typical dose response and stimulation (inset) curves for IR_{50} and pIRIR_{170} signals from sample 153013.

Fig. 5. A. Preheat plateau of IR_{50} from K-feldspar samples. B. Preheat plateau of pIRIR signals from K-feldspar samples. C. Residual doses of IR_{50} signals measured after 4 h exposure in a Hönle SOL2 solar simulator. D. Residual doses of pIRIR signals measured after 4 h exposure in a Hönle SOL2 solar simulator. E. Fading rates (g-value) of IR_{50} signals from sample 153013. F. Fading rates (g-value) of pIRIR signals from sample 153013. G. Dose recovery ratios for IR_{50} signals. H. Dose recovery ratios for pIRIR signals. Open symbols indicate the IR_{50} signal and filled symbols represent the data of the pIRIR signal. Each data point is the mean of three aliquots. Error bars represent the standard error.

1
2
3 *Fig. 6.* Bleaching characteristics of sample 153003. A. Sensitivity-corrected
4 blue-stimulated OSL from quartz, and IR₅₀ and pIRIR₁₇₀ from K-feldspar plotted
5 against bleaching time in a Hönle SOL2 solar simulator. Each data point represents an
6 average of three aliquots. B. Residual dose with solar bleaching time. Each data point
7 represents an average of three aliquots. C. pIRIR₁₇₀ versus IR₅₀ D_e for all the samples.
8 The error bars represent one standard error.
9
10
11
12

13
14 *Fig. 7. A.* Comparison of K-feldspar uncorrected and corrected IR₅₀ ages with quartz
15 OSL ages. B. Comparison between quartz OSL and K-feldspar pIRIR₁₇₀ ages. Note
16 that pIRIR₁₇₀ ages have not been corrected for observed fading (g-values <1%/dec.)
17 as discussed in the text.
18
19
20

21 *Fig. 8. A.* Luminescence and ¹⁴C ages as a function of depth for the Hebei section.
22 Error bars represent one standard error (random component only; i.e. counting
23 statistics, instrument reproducibility). Bayesian fit of the luminescence data below the
24 hiatus is given in blue (1σ error envelope in green) with a depth resolution of 5 cm. B.
25 Calculated MAR values for the Hebei section (red) as a function of luminescence age.
26 Original MAR data for the Xifeng (central CLP; Stevens *et al.* 2016) and calculated
27 MAR data based on Bayesian age-depth model (see Fig. S1). Three-point continuous
28 smoothing has been applied to all Bayesian MAR data.
29
30
31
32
33
34

35 *Fig. 9.* Kernel density estimation of 233 loess-palaeosol ages from 59 sites on the NE
36 Tibetan Plateau (blue curve; kernel bandwidth = 1). The black solid curve represents
37 the average loess deposition flux of the CLP (An *et al.* 1991). Vertical dashed lines
38 show MIS boundaries.
39
40
41
42
43

44 *Table 1.* Summary of sample codes, depths, radionuclide concentrations and dose
45 rates calculated for quartz and K-feldspar. Data in italics and sample codes with
46 asterisk were measured by ICP–MS and converted into Bq kg⁻¹.
47
48
49

50 *Table 2.* Outline of dose measurement protocols used in this study. A. Quartz OSL
51 protocol after (Murray & Wintle 2003). B. Post-IR IRSL protocol modified from
52 Thiel *et al.* (2011) and Buylaert *et al.* (2012). For the ‘natural’ sample, i = 0. The
53
54
55

1
2
3 whole sequence is repeated for several regenerative doses including a zero dose and a
4 repeat dose.
5

6
7 *Table 3.* Summary of quartz OSL and K-feldspar IR₅₀ and pIRIR₁₇₀ equivalent doses
8 and ages. A fading rate of ~2.58%/decade as obtained from sample 153013 is used to
9 calculate the corrected IR₅₀ ages for all the samples. Uncertainties on individual
10 quartz and feldspar ages contain both random and systematic components. Ages (and
11 random errors) in bold have been used for Bayesian modelling in Fig. 8.
12
13

14 15 Supporting Information

16
17
18 Fig. S1. Bayesian fit of the luminescence ages for the Xifeng section published in
19 Stevens *et al.* (2016). Error bars represent one standard error (random component
20 only). Modelled data are shown in blue (1 σ error envelope in green) with a depth
21 resolution of 5 cm.
22
23
24
25
26
27
28
29
30
31
32
33
34
35
36
37
38
39
40
41
42
43
44
45
46
47
48
49
50
51
52
53
54
55
56
57
58
59
60

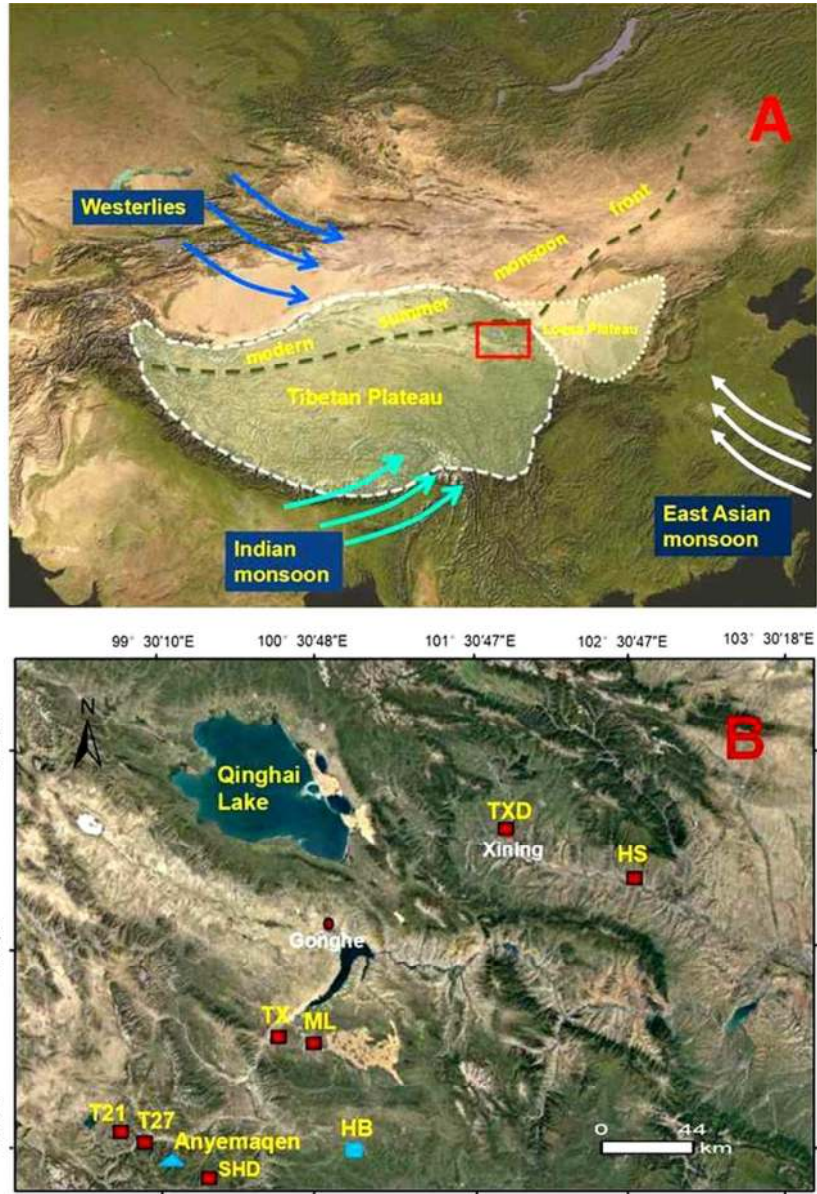


Fig. 1.

147x203mm (120 x 120 DPI)

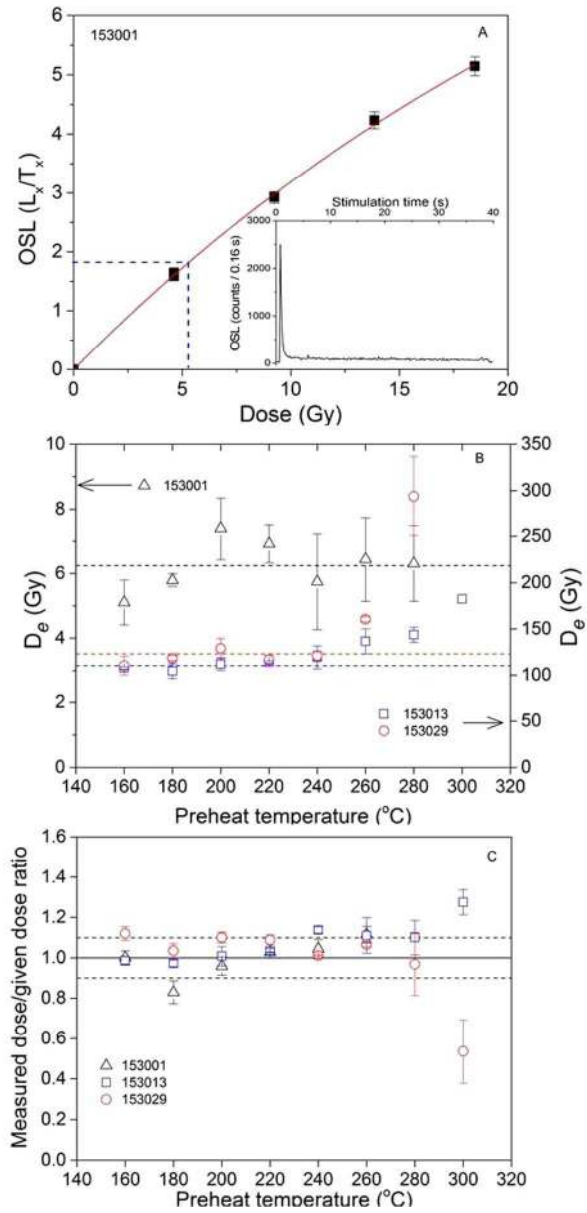


Fig. 2.

135x276mm (120 x 120 DPI)

1
2
3
4
5
6
7
8
9
10
11
12
13
14
15
16
17
18
19
20
21
22
23
24
25
26
27
28
29
30
31
32
33
34
35
36
37
38
39
40
41
42
43
44
45
46
47
48
49
50
51
52
53
54
55
56
57
58
59
60

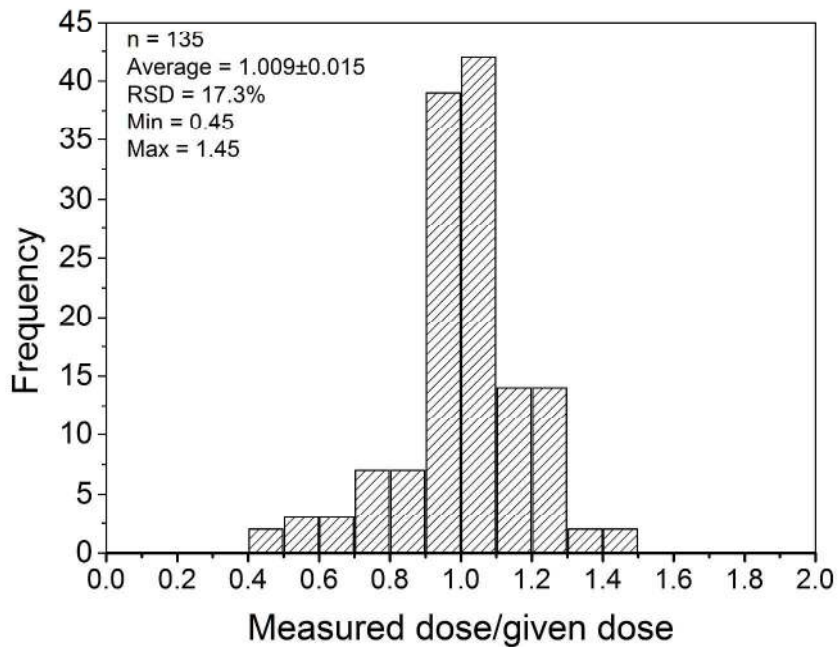


Fig. 3.

279x215mm (300 x 300 DPI)

Only

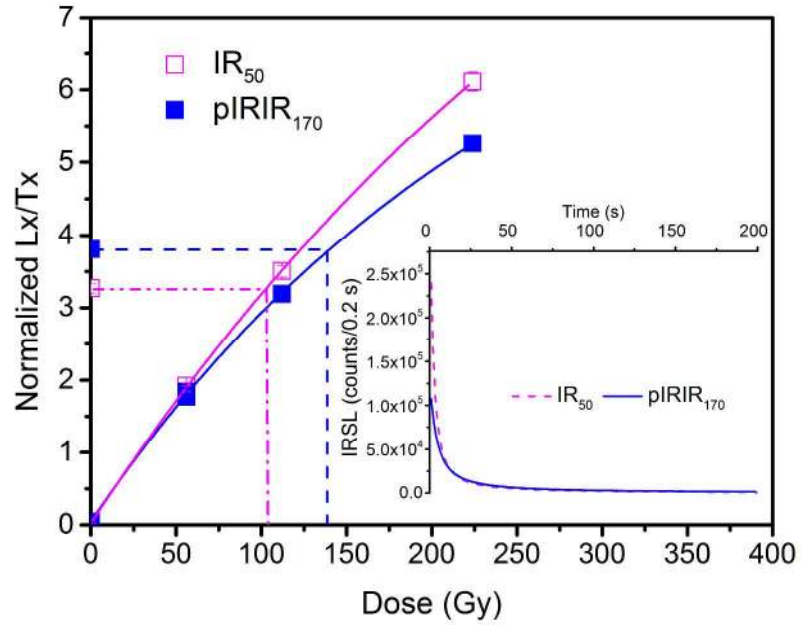


Fig. 4.

296x209mm (300 x 300 DPI)

View Only

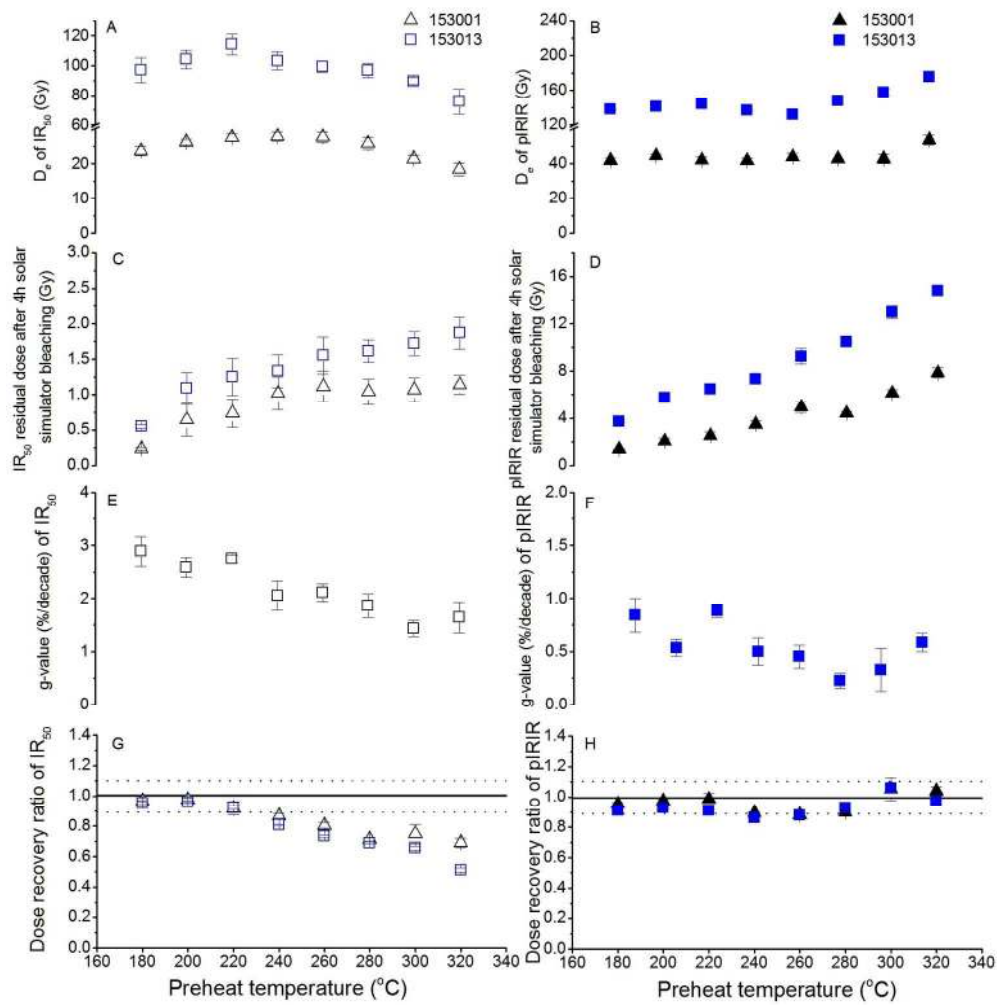


Fig. 5.

394x399mm (120 x 120 DPI)

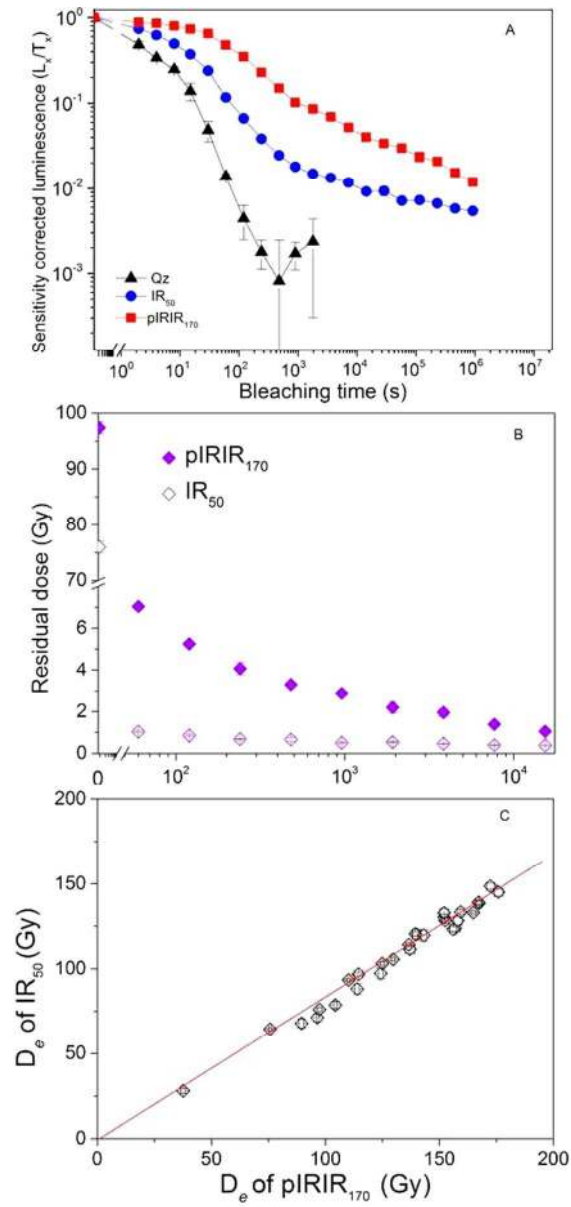


Fig. 6.

121x262mm (120 x 120 DPI)

1
2
3
4
5
6
7
8
9
10
11
12
13
14
15
16
17
18
19
20
21
22
23
24
25
26
27
28
29
30
31
32
33
34
35
36
37
38
39
40
41
42
43
44
45
46
47
48
49
50
51
52
53
54
55
56
57
58
59
60

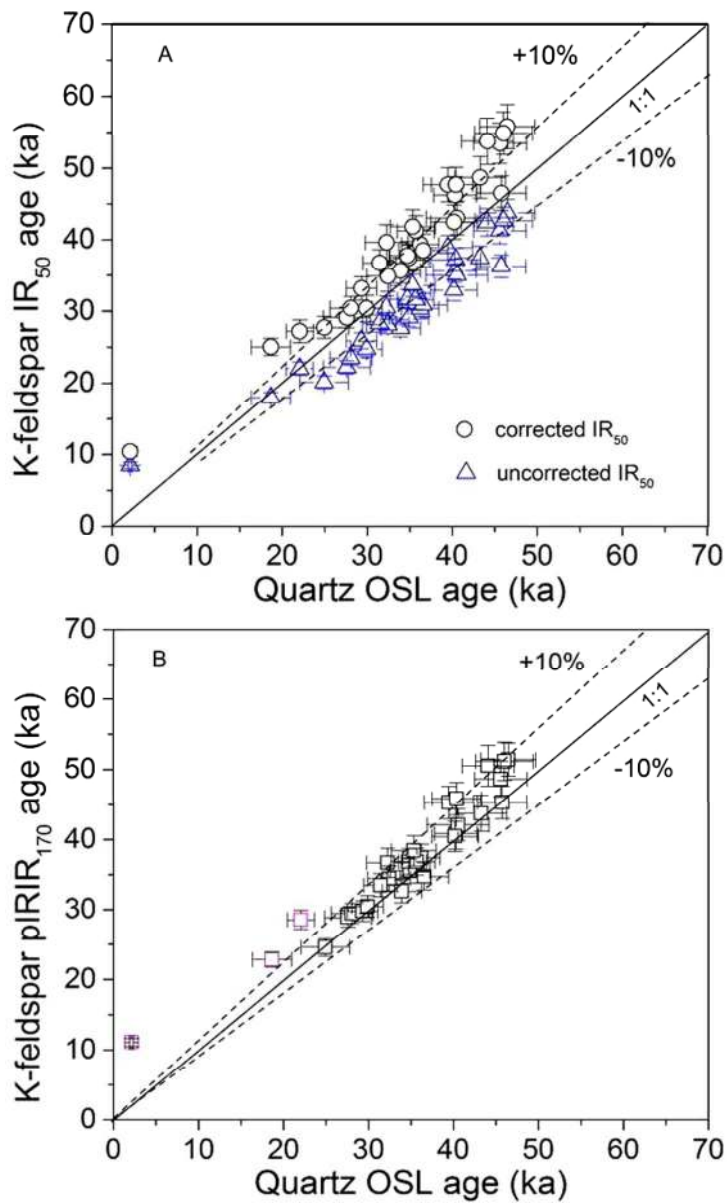


Fig. 7.

135x225mm (120 x 120 DPI)

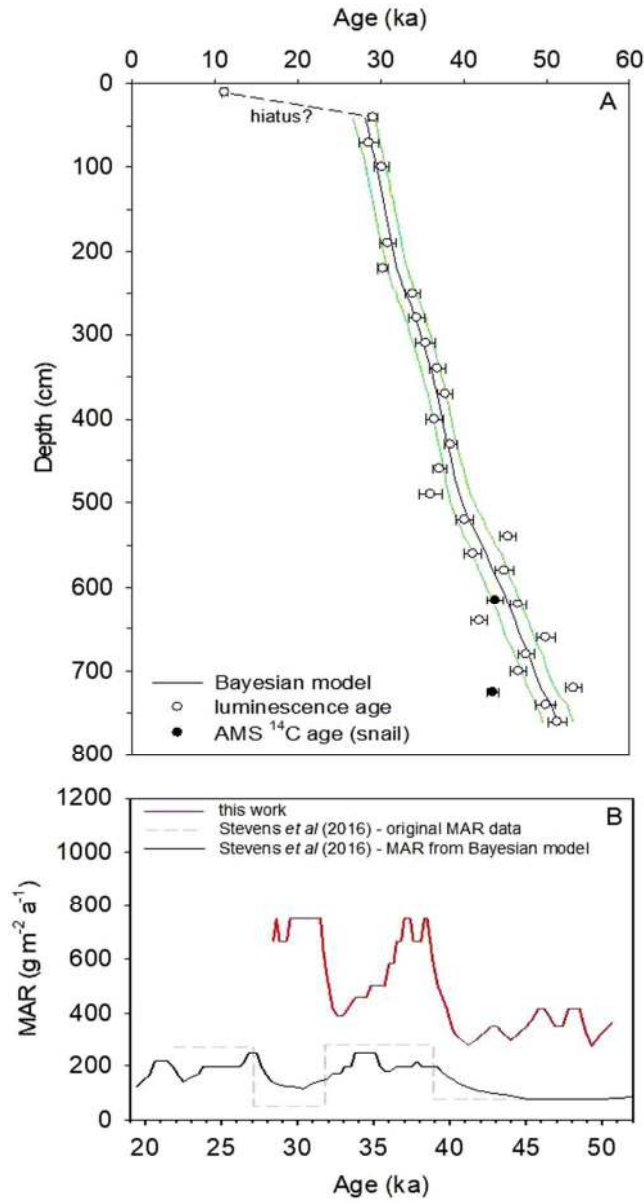


Fig. 8.

117x220mm (120 x 120 DPI)

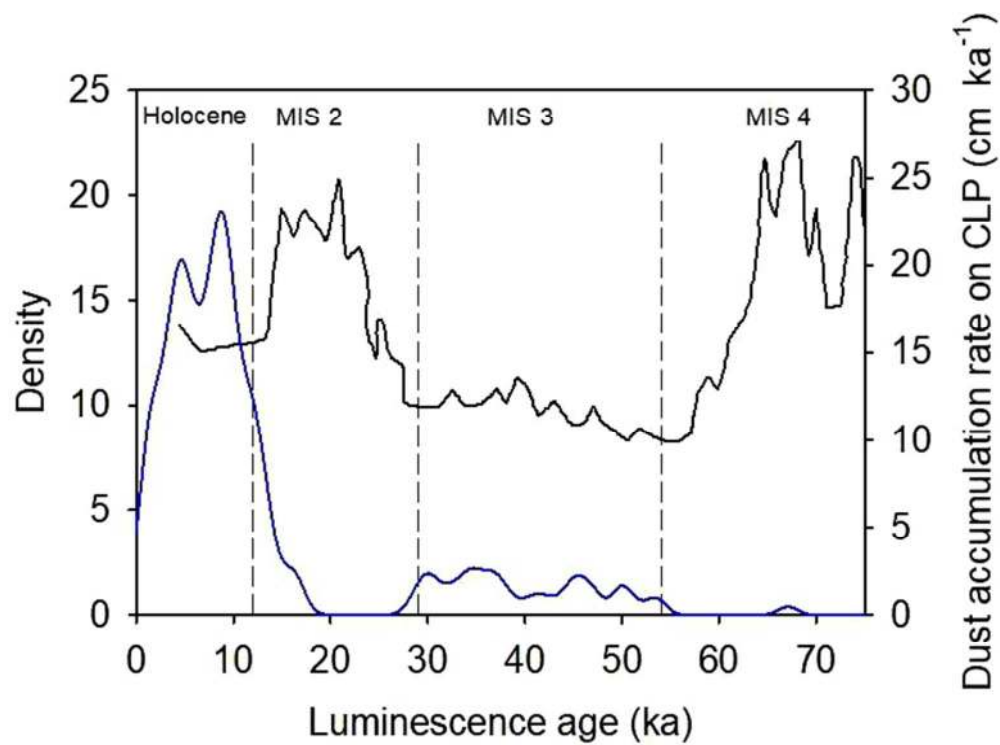


Fig. 9.

152x112mm (120 x 120 DPI)

Sample code	Depth (m)	²³⁸ U (Bq kg ⁻¹)	²²⁶ Ra (Bq kg ⁻¹)	²³² Th (Bq kg ⁻¹)	⁴⁰ K (Bq kg ⁻¹)	Quartz dose rate (Gy ka ⁻¹)	K-feldspar dose rate (Gy ka ⁻¹)
153001	10	29.2±16.5	33.7±1.2	42.1±1.3	459±17	2.99±0.12	3.37±0.13
153002	40	36.2±20.0	30.6±1.1	42.9±1.5	479±20	2.93±0.13	3.32±0.13
153003	70	32.1±15.3	34.4±1.1	41.9±1.1	488±19	2.96±0.13	3.34±0.14
153004*	100	30.6±3.7	-	41.2±2.8	541±13	3.02±0.13	3.40±0.14
153005	130	34.2±12.5	32.1±1.0	40.8±0.9	494±16	3.12±0.13	3.50±0.14
153006*	160	32.6±3.7	-	41.0±2.8	577±13	3.12±0.14	3.50±0.15
153007*	190	36.8±3.7	-	40.7±2.8	572±13	3.15±0.16	3.53±0.15
153008	220	34.5±19.5	37.3±1.5	49.4±1.4	587±25	3.33±0.15	3.72±0.16
153009	250	43.7±17.3	33.9±1.3	42.1±1.4	552±20	3.05±0.13	3.44±0.14
153010	280	36.3±22.2	36.7±1.7	44.0±1.5	577±28	3.19±0.15	3.57±0.16
153011*	310	33.2±3.7	-	42.5±2.8	610±13	3.20±0.14	3.58±0.15
153012	340	48.8±16.8	36.8±1.3	47.2±1.2	563±22	3.19±0.14	3.57±0.15
153013	370	43.3±21.1	38.4±1.6	46.6±1.5	577±27	3.23±0.15	3.62±0.16
153014	400	79.8±28.8	38.7±2.1	49.4±2.0	641±37	3.45±0.17	3.84±0.18
153015*	430	35.0±3.7	-	43.8±2.8	595±13	3.17±0.16	3.56±0.15
153016	460	35.7±21.1	39.0±1.6	51.1±1.5	608±28	3.38±0.16	3.76±0.16
153017	490	42.0±30.3	41.8±2.2	51.5±2.0	631±36	3.48±0.17	3.87±0.18
153018	520	75.9±31.9	41.3±2.3	51.7±2.5	611±33	3.42±0.17	3.80±0.17
153019	540	15.1±23.0	36.8±1.6	44.3±1.8	538±24	3.02±0.14	3.41±0.15
153020	560	37.6±25.4	39.2±1.9	48.9±1.7	605±31	3.32±0.16	3.70±0.17
153021	580	52.5±21.9	36.0±1.6	47.4±1.5	558±28	3.11±0.15	3.49±0.15
153022	620	52.2±19.9	36.7±1.5	41.9±1.6	539±22	2.97±0.14	3.35±0.15
153023	640	31.6±20.6	41.3±1.5	50.0±1.4	619±26	3.39±0.16	3.77±0.16
153024	660	46.6±20.7	33.4±1.5	39.4±1.6	517±23	2.81±0.13	3.19±0.14
153025	680	35.8±18.0	34.8±1.4	44.0±1.3	601±24	3.14±0.14	3.52±0.15
153026	700	44.9±19.0	37.4±1.4	48.0±1.4	571±25	3.15±0.15	3.54±0.15
153027	720	28.6±15.3	32.7±1.1	41.9±1.2	491±16	2.76±0.12	3.14±0.13
153028	740	14.4±29.7	33.0±1.9	43.4±2.1	593±27	3.07±0.15	3.45±0.15
153029	760	28.4±22.8	33.4±1.5	41.5±1.6	594±22	3.04±0.14	3.43±0.15

1
2
3
4
5
6
7
8
9
10
11
12
13
14
15
16
17
18
19
20
21
22
23
24
25
26
27
28
29
30
31
32
33
34
35
36
37
38
39
40
41
42
43
44
45
46
47
48
49
50
51
52
53
54
55
56
57
58
59
60

Step	Quartz OSL	Observed	K-feldspar pIRIR	Observed
1	Regenerative dose, R_i ($i = 0, 1, 2, 3 \dots$)		Regenerative dose, R_i ($i = 0, 1, 2, 3 \dots$)	
2	Preheat (200 °C, 10 s)		Preheat (200 °C, 60 s)	
3			IRSL stimulation (50 °C, 200 s)	$L_{x,IR50}$
4	OSL (125 °C, 40 s)	L_x	IRSL stimulation (170 °C, 200 s)	$L_{x,pIRIR170}$
5	Test dose		Test dose	
6	Cut-heat (160 °C)		Preheat (200 °C, 60 s)	
7			IRSL stimulation (50 °C, 200 s)	$T_{x,IR50}$
8	OSL (125 °C, 40 s)	T_x	IRSL stimulation (170 °C, 200 s)	$T_{x,pIRIR170}$
9	OSL (280 °C, 40 s)		IRSL stimulation (205 °C, 200 s)	
10	Return to step 1		Return to step 1	

FOR Review Only

1
2
3
4
5
6
7
8
9
10
11
12
13
14
15
16
17
18
19
20
21
22
23
24
25
26
27
28
29
30
31
32
33
34
35
36
37
38
39
40
41
42
43
44
45
46
47

Sample no.	Sample name	Depth (cm)	Quartz			K-feldspar								
			D_e (Gy)	Age (ka)	(n)	D_e (Gy)	D_e (Gy)	(n)	Corrected IR ₅₀ age (ka)	Uncorrected pIRIR ₁₇₀ age (ka)	Average age (ka)	Random error (ka)	Total error (ka)	
						IR ₅₀	pIRIR ₁₇₀							
153001	HB01	10	6.6±0.5	2.2±0.2	23	29.5±1	37.6±0.9	12	10.7±0.7	11.2±0.6	-	-	-	-
153002	HB02	40	65.3±3.3	22.3±1.6	22	74.8±0.8	96.4±0.5	12	27.4±1.6	29.1±1.5	-	0.5	-	-
153003	HB03	70	82.7±6.4	28.0±2.6	16	76±1	97.4±1	12	29.3±1.4	29.1±1.4	28.6	1.1	1.8	-
153004	HB04	100	89.2±4.8	29.6±2.2	20	81.7±0.8	104.4±0.6	12	30.6±1.6	30.7±1.5	30.1	0.9	1.8	-
153005	HB05	130	54.1±6.2	17.4±2.2	15	64.4±0.7	75.7±0.6	12	25.2±1.2	21.6±1.1	-	-	-	-
153006	HB06	160	70.0±5.1	22.5±2.0	17	72±1	89.5±1	12	24.9±1.5	25.6±1.3	-	-	-	-
153007	HB07	190	96.1±5.3	30.5±2.3	17	93.4±0.7	110.2±0.7	12	33.3±1.6	31.2±1.6	30.8	0.9	1.8	-
153008	HB08	220	99.5±3.2	29.9±1.9	17	93.6±0.6	113.9±0.9	12	30.5±1.8	30.7±1.6	30.3	0.6	1.6	-
153009	HB09	250	105.1±4.8	34.4±2.4	12	96.8±1	114.6±1.9	12	35.8±1.7	33.3±1.7	33.9	0.9	1.9	-
153010	HB10	280	108.1±5.5	33.9±2.5	20	102.2±1	124.3±0.9	12	35.0±2.1	34.8±1.8	34.3	1.0	2.0	-
153011	HB11	310	115.0±6.7	36.0±2.8	19	103.1±1	124.9±0.9	12	36.9±1.9	34.9±1.7	35.4	1.2	2.1	-
153012	HB12	340	118.9±5.5	37.3±2.6	16	105.6±0.9	129.7±0.8	12	37.6±1.8	36.3±1.8	36.8	1.0	2.1	-
153013	HB13	370	121.6±3.7	37.6±2.4	27	111.5±2.5	137.1±2.1	12	39.5±2.2	37.9±2.0	37.8	0.9	2.1	-
153014	HB14	400	138.9±7.0	40.2±3.1	21	120.2±3	140±1.7	12	38.6±2.3	36.5±2.0	-	1.0	-	-
153015	HB15	430	114.6±2.6	36.1±2.1	24	114.2±0.9	136.6±0.9	12	37.9±2	38.4±1.9	-	0.7	-	-
153016	HB16	460	120.2±3.3	35.6±2.2	11	120.6±1.3	139.5±1.3	12	41.4±2.1	37.1±1.9	-	0.8	-	-

1
2
3
4
5
6
7
8
9
10
11
12
13
14
15
16
17
18
19
20
21
22
23
24
25
26
27
28
29
30
31
32
33
34
35
36
37
38
39
40
41
42
43
44
45
46
47

153017	HB17	490	112.5±5.7	32.3±2.5	11	119.6±3.4	139.2±4.1	11	39.8±2.5	36.0±2.2	-	1.4	-
153018	HB18	520	125.6±5.7	36.8±2.7	16	129.4±1.7	152.5±1.4	12	41.9±2.4	40.1±2.2	-	1.0	-
153019	HB19	540	132.4±3.8	43.8±2.7	13	129.2±1.6	154.4±1.3	12	48.8±2.9	45.3±2.3	-	1.0	-
153020	HB20	560	133.4±3.5	40.2±2.5	13	133.5±1.8	152.1±1.9	12	46.3±2.6	41.1±2.2	-	1.1	-
153021	HB21	580	146.3±11.1	47.1±4.4	11	123.8±1.9	156.8±2.3	12	43.2±2.3	44.9±2.4	-	1.2	-
153022	HB23	620	138.6±4.7	46.7±3.0	15	123.1±1.2	156.1±1.4	15	46.6±2.4	46.6±2.4	-	1.0	-
153023	HB24	640	140.4±5.6	41.4±2.8	12	125.7±1.9	158.1±1.8	15	42.6±2.4	41.9±2.2	-	0.9	-
153024	HB25	660	136.8±7.9	48.7±3.9	11	133.4±1.4	159.3±1.5	12	53.6±2.8	49.9±2.6	-	1.1	-
153025	HB26	680	138.3±10.6	44.1±4.1	11	138.6±1.3	167.4±1.3	12	47.8±2.4	47.5±2.4	-	1.0	-
153026	HB27	700	128.6±6.1	40.8±3.0	10	133.1±0.8	164.9±1	12	47.8±2.4	46.6±2.4	-	1.0	-
153027	HB28	720	142.8±12.4	51.8±5.3	11	139.1±1.2	167.2±1.1	12	55.9±3.1	53.3±2.6	-	1.0	-
153028	HB29	740	132.2±4.4	43.1±2.8	10	148.1±1.6	172.4±1.7	13	53.8±3.2	49.9±2.6	-	1.2	-
153029	HB30	760	135.9±6.6	44.6±3.3	12	147.9±1.5	175.9±1.9	12	55.0±3	51.3±2.6	-	1.1	-

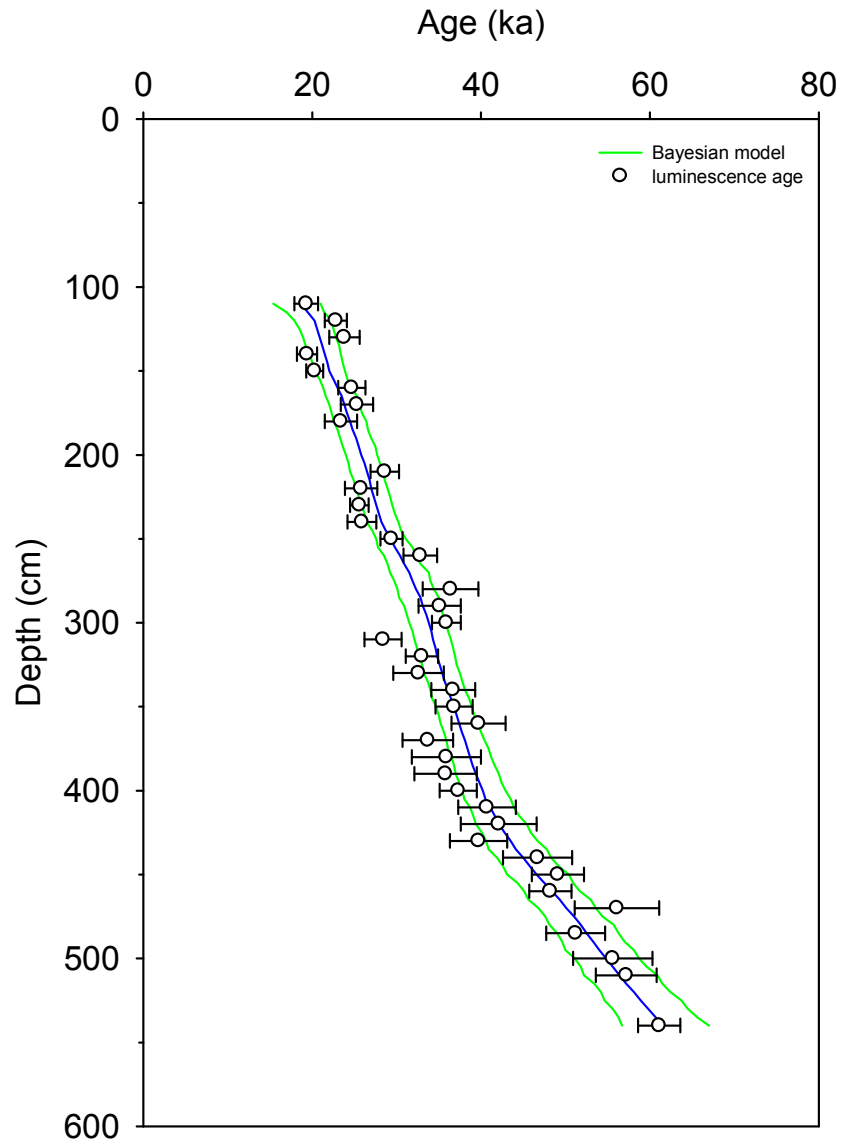


Fig. S1. Bayesian fit of the luminescence ages for the Xifeng section published in Stevens *et al.* (2016). Error bars represent one standard error (random component only). Modelled data are shown in blue (1σ error envelope in green) with a depth resolution of 5 cm.